

13. MINERALOGY AND PETROGRAPHY OF DIAGENETIC DOLOMITE, PERU MARGIN, ODP LEG 201¹

P. Meister,² J.A. McKenzie,² R. Warthmann,² and C. Vasconcelos²

ABSTRACT

Dolomite sampled during Leg 201 occurs as hard lithified layers surrounded by small amounts of friable dolomite, and its presence is related to organic carbon-rich diatomaceous sediments. Petrographic relationships indicate a shallow depth of dolomite precipitation on the Peru margin. Dolomitic breccia layers found on the lower slope, however, were precipitated contemporaneous with brecciation, which probably took place at greater depth under the influence of tectonic deformation processes in the accretionary prism. In most cases, the formation of coexisting framboidal pyrite postdates the growth of dolomite rhombs.

No crystal morphologies indicating a direct influence of bacteria in the precipitation process were observed. Occurrence and morphology of the carbonate layers, however, suggest focused precipitation within the sedimentary sequence. We hypothesize that microbial hot spots discovered during Leg 201 at geochemical boundaries such as the methane/sulfate boundary may be sites of strongly enhanced microbial mediation of dolomite precipitation.

INTRODUCTION

Dolomite is a common feature in organic carbon-rich hemipelagic sediments deposited beneath upwelling zones. Dolomite was recovered during several Deep Sea Drilling Project (DSDP) and Ocean Drilling Program (ODP) cruises in different upwelling systems around the world,

¹Meister, P., McKenzie, J.A., Warthmann, R., and Vasconcelos, C., 2006. Mineralogy and petrography of diagenetic dolomite, Peru margin, ODP Leg 201. In Jørgensen, B.B., D'Hondt, S.L., and Miller, D.J. (Eds.), *Proc. ODP, Sci. Results*, 201, 1–34 [Online]. Available from World Wide Web: <http://www-odp.tamu.edu/publications/201_SR/VOLUME/CHAPTERS/102.PDF>. [Cited YYYY-MM-DD]

²Geological Institute ETH, 8092 Zürich, Switzerland. Correspondence author:

patrick.meister@alumni.ethz.ch

Initial receipt: 7 June 2004
Acceptance: 19 March 2006
Web publication: 11 July 2006
Ms 201SR-102

such as the California margin (DSDP Leg 63), the Gulf of California (DSDP Leg 64), the Oman margin (ODP Leg 117), the Japan Sea (ODP Legs 127/128), and the Namibia margin (ODP Leg 175). This is consistent with observations made in outcrops, such as the Miocene Monterey Formation (California) (e.g., Murata et al., 1969). Because dolomite is usually associated with high organic matter content, an organic dolomite model was proposed (Pisciotta and Mahoney, 1981; Kelts and McKenzie, 1982; Baker and Burns, 1985). The observation that even low amounts of sulfate inhibit the formation of dolomite in high-temperature experiments led to the formulation of the sulfate inhibition model of dolomite formation (Baker and Kastner, 1981). Because pore water sulfate is efficiently removed at sites with increased bacterial sulfate reduction, dolomite can precipitate in association with organic carbon-rich sediments.

Nadson (1928) and Neher and Rohrer (1958) reported precipitation of dolomite in bacterial culture experiments. Vasconcelos and McKenzie (1997) studied a hypersaline coastal lagoon (Lagoa Vermelha, Brazil), a site of modern dolomite precipitation. They formulated a microbial dolomite model, where the presence of active living microbes is essential to overcome the kinetic barrier of dolomite precipitation. Using sulfate-reducing bacteria cultured from Lagoa Vermelha, Vasconcelos et al. (1995) and Warthmann et al. (2000) successfully precipitated dolomite in low-temperature experiments.

The applicability of the sulfate inhibition vs. microbial dolomite model for the formation of deep-sea dolomite remains unresolved, as methods to trace this process in natural environments are limited. A microbial origin may be indicated by crystal morphologies that are similar to round and dumbbell shape crystals produced in culture experiments. Such morphologies were described by Vasconcelos and McKenzie (1997) and van Lith et al. (2003) in sediments from Lagoa Vermelha. Also in this context, it is of interest if dolomite is precipitated as primary precipitate or if a dissolution step of the precursor carbonate is involved (cementation vs. replacement). Bernoulli and Gunzenhauser (2001) and Bernoulli et al. (2004) observed perfect replica structures of diatom frustules in a dolomitized Miocene diatomite layer (Gonfolite Lombarda Group, southern Switzerland) and in pelagic limestone and diatomite of the Romanche Fracture Zone (equatorial Atlantic). These studies showed that deep-sea dolomite is often a primary precipitate, which was formed at an early stage in uncompact sediment. The petrographic relationships of dolomite with sedimentary particles or other diagenetic minerals (e.g., pyrite) provide information about the relative timing of the dolomite precipitation and, therefore, allow correlation with a particular biogeochemical environment.

In this study, we describe and investigate the occurrence, petrography, and mineralogy of dolomite sampled during Leg 201 in deep-sea sediments from the Peru margin. A comprehensive sampling strategy with good depth control of the dolomite occurrences enabled correlation with lithostratigraphic context, pore water chemistry, and microbiology. Leg 201 was the first deep-sea drilling leg dedicated to investigation of a deep seafloor biosphere and was thus an ideal program to study the relation between dolomite formation and deep biosphere activity. The data set produced on board the *JOIDES Resolution* during Leg 201 provides a framework in which to discuss active dolomite precipitation on the Peru margin and to evaluate the environmental factors associated with this process.

Study Area

The Peru margin is a classic site for deep-sea dolomite formation. In the Nazca Plate Project, dolomite was discovered during deep-sea dredging (Kulm et al., 1981b, 1984). These dredge samples provided a good overview of the lateral distribution and occurrence of dolomite. Thornburgh and Suess (1990) studied selected samples of dolostone in order to reconstruct the origin of the pore waters in different parts of the Peru margin.

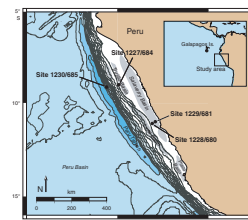
During Leg 201, four sites (all of them redrilled sites of ODP Leg 112) were drilled on the Peru margin (Fig. F1). Sites 1228 (Leg 112 Site 680) and 1229 (Leg 112 Site 681) are located on the Peru shelf at 250 and 150 meters below sea level (mbsl), respectively. Site 1227 (Leg 112 Site 684) was drilled at 430 mbsl on the upper slope of the Peru margin, and Site 1230 (Leg 112 Site 685) was drilled on the lower slope of the Peru Trench (5086 mbsl).

The oceanography of the Peru margin is strongly influenced by southeasterly tradewinds, which cause strong upwelling along the coast of Peru. High productivity leads to an oxygen minimum zone between 150 and 400 mbsl (Suess, von Huene, et al., 1988). Glacial–interglacial sea level variations highly affected sedimentation at the shelf sites. During sea level lowstands, increased rainfall on land delivered higher amounts of siliciclastic material to the basin, upwelling cells migrate seaward, and the oxygen minimum zone impinged farther distal on the seafloor (Suess, von Huene, et al., 1988). Glacial–interglacial cycles are well expressed as variations in sediment composition, total organic carbon (TOC) (Wefer et al., 1990; Meister et al., this volume), and color reflectance (Sites 1228 and 1229) (D’Hondt, Jørgensen, Miller, et al., 2003). Large-scale variations in sediment composition (diatom ooze vs. siliciclastic sediment) correlate with paleobathymetry, based on benthic foraminifers (Resig, 1990), are nonperiodic, and are probably related to tectonic activity. More continuously TOC-rich sediments are present at the lower slope (Site 1230) (Meister et al., this volume).

The tectonic history of the Peru margin was mainly interpreted from the seismic lines acquired during the Nazca Plate Project (Kulm et al., 1981a; Suess, von Huene, et al., 1988). A major hiatus indicates erosion and uplift in the middle Miocene. During this time, hypersaline brine formed under evaporative conditions. Since the late Miocene, the Peru margin has strongly subsided, forming basins and ranges in a forearc basin–type tectonic regime. On the topographic highs, sediment bypass (nondeposition) or erosion occurred, facilitating the recovery of dolomite samples of Miocene age with dredging (Kulm et al., 1981b, 1984), whereas the basins, such as the Salaverry, Lima, and Trujillo Basins, were infilled by continuous sedimentation (Fig. F1). Today, these ancient basins form the shelf and upper slope of the Peru margin. The sediments recovered during Leg 201 on the shelf and upper slope are younger than the middle Miocene hiatus. Paleobathymetry reconstructed by Resig (1990) indicates lower neritic to upper bathyal conditions throughout the Pliocene to Holocene. Therefore, the recovered dolomite is not related to the middle Miocene hypersaline evaporative environment. Tectonic activity at the lower slope is dominated by backthrusting along the accretionary prism, where fluids can be transported upward along the fault zones.

High-resolution pore water chemistry profiles produced during Leg 201 (D’Hondt, Jørgensen, Miller, et al., 2003) indicate different microbial activity in the sediments of the different sites. At the shelf sites,

F1. Leg 201 sites, p. 15.



strongly variable TOC contents appear to be related with penetration depths of sulfate to >30 meters below seafloor (mbsf) (Meister et al., this volume), whereas continuously high TOC of the trench site is reflected in removal of sulfate at 7 mbsf and the presence of gas hydrates. Evaporative brine, present at the shelf sites, delivers electron acceptors from beneath. Different microbial activities as well as cell concentrations (D'Hondt, Jørgensen, Miller, et al., 2003) are the result of these special biogeochemical conditions, but microbial activity also influences the pore water chemistry and, therefore, may control the formation of dolomite at the different sites.

METHODS

Dolomite nodules and layers were systematically sampled onboard the *JOIDES Resolution* during Leg 201. A comparison sample was taken from the surrounding soft sediment with each dolomite sample. Thin sections were stained for calcite according to the method of Dickson (1966) and analyzed using a petrographic microscope. For description of crystallization textures and fabrics of dolomite, the terminology of Friedman (1965) was used. Additionally, cold cathode luminescence was applied in order to detect different generations of carbonate cements.

Bulk dolomite nodules and surrounding sediment samples were powdered and mineralogically analyzed using a Scintag XDS 2000 X-ray diffractometer (XRD). The samples were scanned continuously at 1°/min from 10° to 70° with CuK α radiation. Dolomite stoichiometry was calculated from displacement of the (104) peak using the equation of Lumsden (1979).

Fresh broken surfaces of lithified dolomite, as well as samples of freeze-dried unlithified sediment, were coated with platinum and analyzed by field emission scanning electron microscope (SEM; LEO 1530, 143-eV resolution; LEO Electron Microscopy Ltd., Germany) at the Institute for Material Sciences at ETH Zürich (Switzerland). Phase compositions were measured using energy dispersive X-ray (EDX; Z-MAX 30-UP; Thermo NORAN). The acceleration voltage was set at 5 kV for microscopy and at 10 kV for EDX analysis.

Major elements (Mg, Ca, Fe, Mn, and Sr) in the dolomite phase were quantified by electron microprobe analysis (EMPA). All samples were polished (thin sections, as well as embedded rock pieces) and coated with a 20-nm-thick carbon layer before being analyzed on a Cameca SX 50 electron microprobe at the Institute for Mineralogy and Petrography at ETH Zürich. Acceleration voltage was set to 15 kV. A variety of carbonate standards from the ETH Zürich collection were used: calcite (E001), magnesite (E004), siderite (E006), rhodochrosite (E003), and strontianite (E012). Ca and Mn were analyzed using penta-erythritol (PET) crystal, Mg and Sr using thallium acid phthalate (TAP), and Fe using lithium fluoride (LIF). PET, TAP and LIF are three different crystals with different 2d values used for monochromizing. Textural relationships between the phases were studied using reflected light microscopy. Carbon (as carbonate) was calculated by stoichiometry. A total of 50 measurements were taken from each sample with 7-nA probe current and a spot size of 5 μ m. Because of the small grain size of the micritic carbonate, only large crystals were measured.

STRATIGRAPHY, PETROGRAPHY, AND MINERALOGY

Upper Slope Site 1227/684

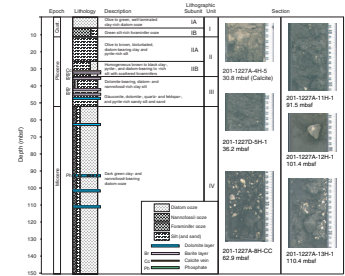
Site 1227 (redrilled Site 684) was drilled on the upper slope of Peru margin at 430 mbsl. A 150-m-thick middle Miocene to Holocene condensed section of the distal Trujillo Basin was recovered (Fig. F2). Below 12 m of Quaternary diatom and foraminiferal ooze, Pliocene mixed diatomaceous and siliciclastic sediment is present. A 5-m-thick, coarse, pyrite-rich glauconitic sand marks the base of the Pliocene at 50 mbsf. Both the foraminiferal ooze and the glauconite sand are well sorted and coarse grained and seem to be the result of winnowing. Also, both horizons are characterized by low TOC, high natural gamma radiation, and high magnetic susceptibility, which is indicative of condensed sections and may contain erosional surfaces or even major unconformities. These horizons correlate with the Miocene/Pliocene and Pliocene/Pleistocene boundaries. Below the lower horizon, the drilled section comprises Miocene diatom ooze. Horizons of phosphatic pebbles as much as 2 cm across are often intercalated in these sediments. The pebble layers caused poor recovery because they were not washed out by the drilling fluid, but, as the foraminifer and glauconite sand layers, they show high natural gamma radiation and magnetic susceptibility and probably also represent condensation or erosion surfaces. The pebbles consist of hard phosphate and dolomite, which was probably eroded from hardgrounds and/or diagenetically formed layers and were concentrated by winnowing and rounded on the seafloor (cf. Monterey Formation; Garrison and Graham, 1984). These condensation horizons punctuate the reduced stratigraphy at Site 1227.

More than 10 carbonate pieces were logged at Site 1227; most occurred as reworked pebble layers, but in situ layers were also found (Fig. F2). Between 30 and 50 mbsf, massive 2-cm-thick barite layers were found, whereas dolomite layers were mostly found in the underlying Miocene diatom ooze. Pebbles are gray to very light gray or yellowish. In general, they are densely lithified, but some semilithified pieces were also present. At 31 mbsf, a fragment of a 0.5-cm-thick, white calcite layer was observed.

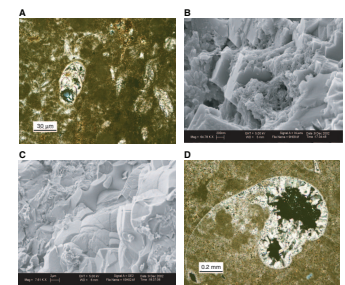
Inhomogeneous microsparitic dolomite (Pl. P1A) consists of micron-to decimicron-scale euhedral rhombs with “stairlike” structures (Pl. P1B), whereas larger xenotopic crystals were observed in cements (Pl. P1C). Abundant, mostly benthic foraminifers are often infilled with coarse fringe cement and a later generation of blocky dolomite cement (Pls. P1C, P1D, P2A). Diatom frustules are also often infilled with dolomite cement (Pl. P2B). Some dolomites are more friable and show a high porosity. Most cavities are elongated and follow lamination. They are surrounded by rims of calcite microsparite or dolomicrosparite (similar to Pl. P6A), suggesting the cavities were already present during the time of cementation. Framboidal pyrite is seen growing in the empty space inside a diatom frustule (Pl. P2C). In a few cases, almost fossil-free detrital quartz was observed being cemented by dolomicrosparite.

XRD mineralogy analysis revealed very well ordered dolomite slightly enriched in calcium (Fig. F3). Using the equation of Lumsden (1979), CaCO₃ contents of 52–56 mol% were calculated for the dolomite phase. Calcite is always present in low amounts, probably as a result of marine sedimentary calcite. Luminescence is generally strong

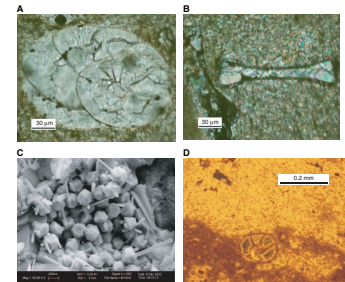
F2. Lithostratigraphic profile, Site 1227/684, p. 16.



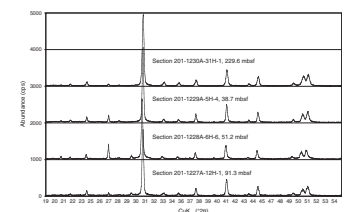
P1. Foraminifers in dolomitic groundmass, p. 22.



P2. Foraminiferal test, Site 1227, p. 23.



F3. X-ray diffractograms, p. 17.



Quaternary laminated diatom ooze with a siliciclastic zone between 40 and 100 mbsf. Several condensation horizons and/or erosion surfaces with phosphate nodules were found (Shipboard Scientific Party, 2003), often at the base of 10-m cycles (glacial–interglacial cycles) (Wefer et al., 1990; Meister et al., this volume). Below 130 mbsf, Pliocene and Pleistocene well-sorted feldspar quartz sands are present.

Dolomite layers are most abundant at Site 1229 (Fig. F5), concentrated around 30 and 100 mbsf. Below 130 mbsf, dolomite is rare in the siliciclastic Pliocene–Pleistocene sediments. Dolomite occurrence is correlated with the beginning of upwelling-related sedimentation at ~140 mbsf and occurs generally in zones with high TOC and high bacterial cell numbers (cf. D’Hondt, Jørgensen, Miller, et al., 2003). Dolomite occurs as 3-cm-thick layers, which mostly show flat bottoms and tops and appear to be part of continuous layers cut by advanced piston coring. Lamination parallel to the top and bottom of the layer was observed in most of the samples. Typically, relatively hard and dense laminae are interlayered with soft, porous 0.5-cm-thick laminae. The color is mostly yellowish light gray, but a few layers are light gray. The nodules are surrounded by friable dolomite.

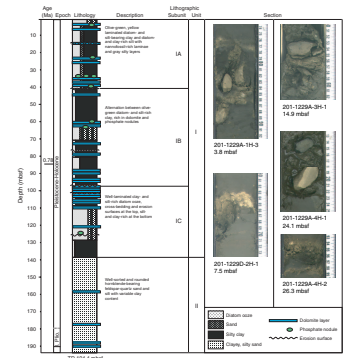
The hard layers consist of a homogeneous microsparitic groundmass of decimicron-scale euhedral dolomite rhombs. The grain size is coarser around cavities and fossils. Veins and irregular cavities oriented parallel to the lamination and surrounded by fine microsparitic seams were found in the friable laminae (Pl. P6A). They are probably a result of incomplete cementation. Large 50- μ m crystals showing edged surfaces were found in a dolomite layer at 7.5 mbsf, associated with well-preserved diatoms (Pl. P6B). A few samples are rich in well-sorted angular quartz grains, reflecting the composition of the surrounding sediment.

Foraminiferal tests are rare at Site 1229. They often show a fringe of fibrous calcite cement, which is partially replacing the original test. The cavity is partially filled with blocky dolomite cement, which postdates the formation of the fibrous cement (Pl. P6C, P6D). These generations are clearly revealed by cathode luminescence (Pl. P7A, P7B, P7C). SEM images (Pl. P8A, P8B, P8C, P8D) show the foraminiferal tests to be covered by perfectly euhedral decimicron-scale dolomite rhombs. They are oriented exactly along the surface of the test and replicate the pore pattern of the foraminiferal test. Framboidal pyrite fills the empty pore space between the dolomite rhombs and, therefore, postdates the growth of the rhombs (Pl. P9A, P9B).

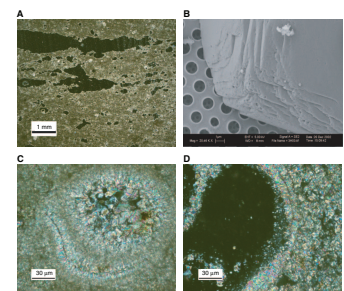
Diatoms are very abundant and occur in diverse shapes at Site 1229 (Pl. P9C, P9D). They are well preserved and enveloped by euhedral dolomite rhombs, which replicate the pore pattern of the diatom. Dolomite grows into the round pores of the diatom frustules (Pl. P10A, P10B, P10C, P10D). A siliceous skeletal fragment found at 99 mbsf (Pl. P11A) is strongly corroded and seems to be less stable than the other surrounding diatom frustules, which appear to be very well preserved. A dolomite rhomb grew beneath but did not infill all of the space between the pores and probably stopped growing when the siliceous frustule still was being corroded.

Thin section staining is mostly colorless, reflecting the dolomitic mineralogy of the sample. In all samples, well-ordered dolomite was determined to be the major component by XRD analysis (Fig. F3). Calcite occurs only in trace amounts except in the uppermost 15 m, where higher calcite levels might be due to higher percentages of nanofossils in the sediment. In one sample that contained a centimeter-scale bivalve shell, high-Mg calcite was detected. The Ca content calculated

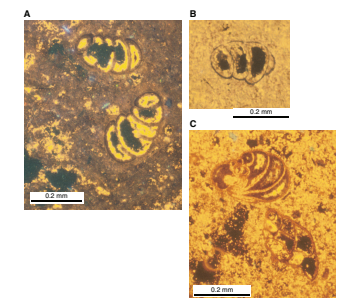
F5. Lithostratigraphic profile, Site 1229/681, p. 19.



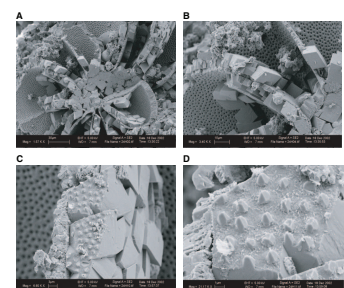
P6. Elongate pores, p. 27.



P7. Calcitic foraminiferal test, p. 28.



P8. Perforate foraminiferal test, p. 29.



from XRD using the equation of Lumsden (1979) ranges from 50 to 55 mol%. The slight enrichment of Ca in the dolomite phase was also observed by EMPA. Cathode luminescence shows yellow to orange with brighter luminescence in the coarser areas.

Peru Trench Site 1230/685

On the lower slope of the Peru Trench (5086 mbsl), 280 m of sediment was penetrated (Fig. F6), and >200 m of Pleistocene–Holocene black diatom ooze with variable amounts of siliciclastic material was recovered. This thickness is greater than that in the depocenter on the shelf. Below a major fault at 216 mbsf, Miocene diatom-rich and siliciclastic sediments with low TOC content are present. Sulfate is consumed from the pore water within the uppermost 7 mbsf; below 10 mbsf, signs of degassing (gas bubbles) were recognized. This site shows high methanogenic activity and stability of gas hydrates (D’Hondt, Jørgensen, Miller, et al., 2003).

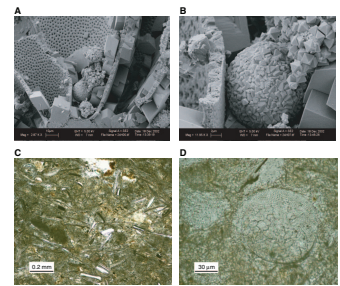
Sediments from the lower slope of the Peru margin are highly affected by downslope mass movements that caused centimeter-scale high-angle normal faults and ductile slumping (Kemp and Lindsley-Griffin, 1990). Below 200 mbsf, sediments show increased compaction and stiffness and pervasive cleavage. Disruption and brecciation is common. These deformation structures are due to a compressional regime and underthrusting along the accretionary prism (Kemp and Lindsey-Griffin, 1990).

Carbonate precipitates are rare at Site 1230. Several dolomite layers were identified at ~230 mbsf (Fig. F6), but more were found at deeper levels during Leg 112 drilling (Thornburg and Suess, 1990). A 3-cm-thick dolomite layer was also sampled in a diatom ooze at 6 mbsf during Leg 112. At 229 mbsf, an 18-cm-thick hard lithified dolomite breccia layer was recovered at Site 1230. Breccia layers such as this are common at greater depths and are ascribed to the tectonic activity of the accretionary prism. Disseminated dolomite only occurs in the neighborhood of hard, lithified layers.

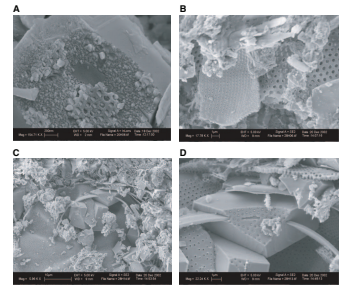
Dolomite breccias consist of clasts of subhedral dolomicrite (Pl. P11B, P11C). Between the clasts, cement often shows xenotopic 10- to 50-µm texture with the grains developing compromise boundaries (Pl. P12A, P12B, P12C, P12D). A fossil found at 229 mbsf is completely replaced by dolomite (Pl. P13A, P13B). The central cavity is filled with pyrite, which was precipitated after dolomitization. Fossils are rarely found in these hard dolomite layers; only a few angular quartz grains are present.

Cathode luminescence revealed several generations of sediment infill and cementation between the clasts (Pl. P13C, P13D). The clasts are surrounded by a yellow luminescent rim that clearly separates dolomite generations older and younger than brecciation. Dolomitization of the clasts with relatively low luminescence and zonation predates deformation. Each deformation event was followed by a new generation of strongly luminescent cement. In general, later generations are more luminescent. A central cavity is visible in Plate P13D. Precipitates of a dark, fine-grained mineral could not be identified by morphology, but blue staining of thin sections indicates the presence of iron. As iron could not be detected by EMPA in the dolomite phase, it probably represents pyrite precipitated in the cavity during a later phase of diagenesis. Dolomite analyzed by XRD is well ordered and contains 51–53

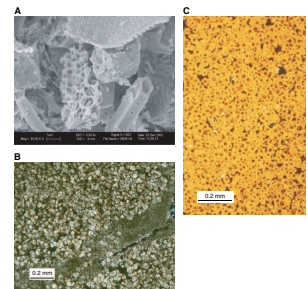
P9. Pyrite framboids, p. 30.



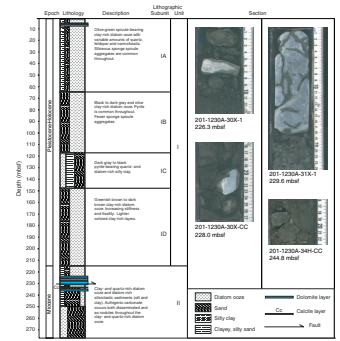
P10. Dolomite in diatom frustules, p. 31.



P11. Skeletal fragment, p. 32.



F6. Lithostratigraphic profile, Site 1230/685, p. 21.



mol% calcium carbonate (Fig. F3). EMPA confirms the enrichment of calcium in the dolomite phase.

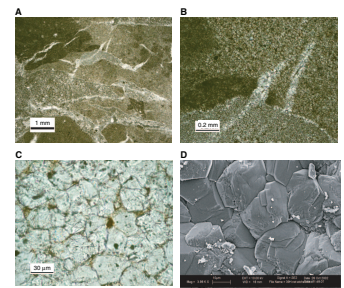
DISCUSSION

During Leg 201, two different types of dolomite with different morphologies and depths of precipitation were found in the Peruvian shelf sediments and in the trench. All recovered dolomites were formed in lower neritic to abyssal sediments and not shallow-marine evaporative conditions, as shown by paleobathymetry determined from benthic foraminifers (Resig, 1990). Older dolomites were recovered by dredging (Kulm et al., 1984) or deeper drilling during Leg 112 (Thornburg and Suess, 1990), and some of them were shown to be formed in evaporitic basins in the Miocene, when the brine also formed.

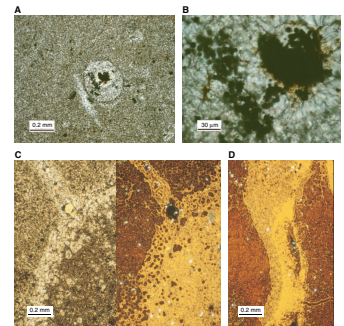
Peru Margin Dolomites

At all sites drilled on the Peru margin during Leg 201, dolomite layers were recovered in sediments formed under upwelling conditions. They are 2–5 cm thick, laminated, and densely lithified. Friable dolomite is rare, but it does occur around hard layers and rarely as single laminae. It is never homogeneously distributed in the sediment column. The fine-grained and homogeneous dolomicrosparite consists of micron- to decimicron-size euhedral rhombs. Only small amounts of possible precursor carbonate are present in the sediment, and dolomite forms as a primary precipitate. Foraminiferal tests and diatom frustules are well preserved and not replaced but cemented by the growing diagenetic dolomite. Foraminifers show growth of fibrous calcite cement at different sites. This cement formed before dolomite growth and also shows evidence of dolomitic replacement. Often, dolomite rhombs appear as replicas of the porous surface of the foraminiferal tests and the diatom frustule. However, the pores of a strongly dissolved siliceous frustule at Site 1228 are not completely filled with dolomite. The formation of framboidal pyrite postdates dolomite formation. This indicates that the dolomitization process was terminated early. The youngest dolomite layers often appear between 10 and 30 mbsf; most are probably formed in this depth range, where the uncompacted diatomaceous sediments still have a high porosity. This observation is in agreement with observations from other environments, such as the Miocene dolomite-cemented diatomite layer in the Southern Alpine Gonfolite Lombarda Group (Bernoulli and Gunzenhauser, 2001). Dolomite layers show similar size and shape within each site, but they are different between the sites. Cementation style is also characteristic for each site. This indicates that the discrete dolomite layers probably formed under the same conditions at each site. Results from XRD and EMPA show that all Peru margin dolomites have a well-ordered stoichiometry with a slight enrichment in calcium. Dolomite layers are not always correlated with diatomaceous horizons, thus not directly depend on lithology. However, on a broad scale, dolomite only occurs in sediments associated with the upwelling zone. Because they occur as distinct layers, dolostones in the Peru margin probably formed along a sharp geochemical interface relatively early in the sedimentary column. An early precipitation (i.e., in the uppermost 30 mbsf) is also suggested by Sr isotopic composition similar to seawater values and the disequilibrium of $\delta^{13}\text{C}$ of the dolomite with $\delta^{13}\text{C}$ in dissolved inorganic carbon of modern pore water

P12. Dolomite breccia, p. 33.



P13. Strongly replaced fossil, p. 34.



(M.L. Musgrove and D. Schrag, pers. comm., 2004; and P. Meister, unpubl. data). A possible interface would be the boundary between the sulfate-reducing and methanogenic diagenetic zones. At this interface, sulfate ions, proposed as a kinetic inhibitor (Baker and Kastner, 1981), are removed and alkalinity reaches peak values (D'Hondt, Jørgensen, Miller, et al., 2003), whereas Mg and Ca concentrations simultaneously decrease at these depths (Suess, von Huene, et al., 1988). Also, these interfaces (in particular at Site 1229) seem to be hot spots of microbial activity (D'Hondt, Jørgensen, Miller, et al., 2003) and, therefore, may play an important role in dolomite formation. Carbon-13 values of the dolomite layers are strongly variable, but fall into the range of values measured in the dissolved inorganic carbon at the sulfate/methane interface.

Peru Trench Dolomites

Dolomite layers found below 200 mbsf in the Peru Trench are strongly brecciated and consist of centimeter-scale clasts with planar subhedral dolomite grains overgrowing the original sediment. Remnants of marine calcitic organisms are almost completely replaced by the coarse anhedral dolomite. Xenotopic textures are nicely developed in the matrix as a result from simultaneous growth of neighboring crystals along compromise boundaries. Simultaneous growth is only possible if the dolomitizing fluid is strongly supersaturated with respect to dolomite. Cathode luminescence revealed several generations of dolomitic cement formed in the open spaces between the clasts contemporaneously with the brittle deformation. Open pore spaces are partially filled with soft sediment and partially filled with coarse sparitic dolomite and a central cavity. The last phase of diagenesis ended with the precipitation of fine-grained pyrite.

Dolomite mineralization is strongly related to brecciated layers, which were observed also in several deeper layers during Leg 112. The brittle deformation has been related to shear zones within the accretionary prism, which only occur at depths deeper than 200 mbsf. Therefore, the synkinematic precipitation of dolomite occurred not early in the sedimentary column but more deeply buried, in compacted sediment. The stiffness of the compacted sediment, and perhaps also the presence of gas hydrates, are responsible for the brittle behavior and preferential deformation along discrete fault zones, where hard lithified dolomite was brecciated. Most likely these shear zones provide fluids from deeper parts of the accretionary prism that enhance precipitation of dolomite. Last-stage precipitation of high amounts of pyrite supports the presence of a sulfidic species in the pore water. So far, neither the microbial model (mediation through enhanced microbial activity along the fluid conduits) nor any abiogenic model (e.g., rapid fluid decompression) can be excluded for the formation of the dolomite breccias.

Controlling Factors

The fact that dolomite occurs as hard lithified layers and not continuously as disseminated rhombs, as in the Monterey Formation, which experienced higher temperature diagenesis (Isaacs, 1984), indicates that dolomite precipitation is not a continuous process but probably forms at distinct geochemical interfaces. This also explains why dolomite layers form in different horizons with different sediment composition and porosity but on a large scale related to organic carbon-rich upwelling

sediment. An analog example could be barite layers that formed at the boundary between the methanogenic and the sulfate-reduction zone (Site 1227) (D'Hondt, Jørgensen, Miller, et al., 2003) and show morphologies very similar to the dolomite layers. For dolomite formation, Mg and Ca concentrations in the pore water (Suess, von Huene, et al., 1988) are not the controlling factors, as these ions become depleted at the depth of dolomite formation, but the consumption of sulfate and an increase of alkalinity are important controls. Dolomite precipitation at the methane/sulfate interface, where sulfate is completely consumed by sulfate-reducing bacteria, would be consistent with the sulfate inhibition model. Crystal morphologies typical for microbially mediated dolomite, as observed in culture experiments and in the natural environment (Lagoa Vermelha), were not found in the deep-sea sediments. This study, however, provides evidence that dolomite formation occurs at depths, where microbial cell concentration and activity (Shipboard Scientific Party, 2003) are high, suggesting the relevance of the microbial dolomite model in this deep-sea environment. Microbial activity is enhanced at biogeochemical interfaces where high gradients in ion concentration can be used as an energy source. At the same time, these interfaces are maintained by the bacteria and represent zones with ion concentrations suitable for dolomite precipitation.

CONCLUSION

Formation of dolomite layers was observed in organic carbon-rich upwelling-related sediments of the shelf and upper slope of the Peru margin. Dolomite forms early as a primary precipitate in uncompact sediment and is not replacing the precursor carbonate. These findings, together with the results of an isotopic study (Meister et al., unpubl. data; see discussion above), are consistent with a model for dolomite formation associated with a biogeochemical interface, such as the methane/sulfate boundary. Dolomite breccias were precipitated on the lower slope of the Peru margin contemporary with the brittle deformation along faults in the accretionary prism. These dolomites were formed in association with hydrothermal fluid flow. The presence of great amounts of pyrite indicates the in situ reduction of sulfur species and thus, dolomite formation in the fault zones may also be related to microbial activity.

Even though no crystal morphologies typical for microbially mediated carbonates were found, the dolomite formation is probably related to zones of increased microbial activity in support of the microbial dolomite model. This activity provides high alkalinity and removes sulfate from the pore water, which would be consistent with the sulfate inhibition model. Thus, for the Peru margin environment, dolomite formation may be promoted by both microbial mediation and sulfate depletion. Further geochemical and isotopic studies are required in order to determine the major control on deep-sea dolomite formation.

ACKNOWLEDGMENTS

This study is based on SEM imaging assisted by Brandon Bürgler and petrographic thin sections prepared by Margrit Bischof and Frowin Pirovino. We also acknowledge Eric Reusser for helping with the EMPA. Daniel Bernoulli inspired this study with his insights regarding replica

structures on dolomite crystals. We thank him, Robert Garrison, and Lorri Peters for carefully reviewing this manuscript. Thanks also to the Leg 201 Shipboard Scientific Party for helping to acquire the dolomite samples. This research used samples and data provided by the Ocean Drilling Program (ODP). ODP is sponsored by the U.S. National Science Foundation (NSF) and participating countries under management of Joint Oceanographic Institutions (JOI), Inc. This study was partially financed by Swiss National Fund (SNF) project numbers 20-59282 and 20-67620. The SNF also sponsors the Swiss participation in ODP.

REFERENCES

- Baker, P.A., and Burns, S.J., 1985. The occurrence and formation of dolomite in organic-rich continental margin sediments. *AAPG Bull.*, 69:1917–1930.
- Baker, P.A., and Kastner, M., 1981. Constraints on the formation of sedimentary dolomite. *Science*, 213:215–216.
- Bernoulli, D., Gasperini, L., Bonatti, E., and Stille, P., 2004. Dolomitization in pelagic limestone and diatomite, Romanche Fracture Zone, equatorial Atlantic. *J. Sediment. Res.*, 74:180–188.
- Bernoulli, D., and Gunzenhauser, B., 2001. A dolomitized diatomite in an Oligocene–Miocene deep-sea fan succession, Gonfolite Lombarda group, northern Italy. *Sediment. Geol.*, 139:71–91. doi:10.1016/S0037-0738(00)00159-7
- Dickson, J.A.D., 1966. Carbonate identification and genesis as revealed by staining. *J. Sediment. Petrol.*, 36:491–505.
- D’Hondt, S.L., Jørgensen, B.B., Miller, D.J., et al., 2003. *Proc. ODP, Init. Repts.*, 201 [CD-ROM]. Available from: Ocean Drilling Program, Texas A&M University, College Station TX 77845-9547, USA. [HTML]
- Friedman, G.M., 1965. Terminology of crystallisation textures and fabrics in sedimentary rocks. *J. Sediment. Petrol.*, 35:643–655.
- Garrison, R.E., and Graham, S.A., 1984. Early diagenetic dolomites and the origin of dolomite-bearing breccia, Lower Monterey Formation, Arroyo Seco, Monterey County, California. In Garrison, R.E., Kastner, M., and Zenger, D.H. (Eds.), *Dolomites of the Monterey Formation and Other Organic-Rich Units*. Spec. Publ.—Soc. Econ. Paleontol. Mineral., 41:87–102.
- Isaacs, C.M., 1984. Disseminated dolomite in the Monterey Formation, Santa Maria and Santa Barbara areas, California. In Garrison, R.E., Kastner, M., and Zenger, D.H. (Eds.), *Dolomites of the Monterey Formation and Other Organic-rich Units*. Spec. Publ.—Soc. Econ. Paleontol. Mineral., 41:155–169.
- Kelts, K., and McKenzie, J.A., 1982. Diagenetic dolomite formation in Quaternary anoxic diatomaceous muds of Deep Sea Drilling Project Leg 64, Gulf of California. In Curray, J.R., Moore, D.G., et al., *Init. Repts. DSDP*, 64 (Pt. 2): Washington (U.S. Govt. Printing Office), 553–569.
- Kemp, A.E.S., and Lindsley-Griffin, N., 1990. Variations in structural style within Peruvian forearc sediments. In Suess, E., von Huene, R., et al., *Proc. ODP, Sci. Results*, 112: College Station, TX (Ocean Drilling Program), 17–31.
- Kulm, L.D., Dymond, J., Dasch, E.J., and Hussong, D.M. (Eds.), 1981a. *Nazca Plate: Crustal Formation and Andean Convergence*. Mem.—Geol. Soc. Am., 154.
- Kulm, L.D., Suess, E., and Thornburg, T.M., 1984. Dolomites in the organic-rich muds of the Peru forearc basins: analogue to the Monterey Formation. In Garrison, R.E., Kastner, M., and Zenger, D.H. (Eds.), *Dolomites in the Monterey Formation and Other Organic-rich Units*. Spec. Publ.—Soc. Econ. Paleontol. Mineral., 41:29–48.
- Kulm, L.D., Thornburg, T.M., Schrader, H., Masias, A., Resig, J.M., and Johnson, L., 1981b. Late Cenozoic carbonates on the Peru continental margin: lithostratigraphy, biostratigraphy, and tectonic history. *Mem.—Geol. Soc. Am.*, 154:469–508.
- Murata, K.J., Friedman, I., and Madsen, B.H., 1969. Isotopic composition of diagenetic carbonates in marine Miocene formations of California and Oregon. *USGS Prof. Paper*, 614-B:24.
- Lumsden, D.N., 1979. Discrepancy between thin section and X-ray estimates of dolomite in limestone. *J. Sediment. Petrol.*, 49:429–436.
- Nadson, G.A., 1928. Beitrag zur kenntnis der bakteriogenen kalkablagerungen. In Thienemann, A.U.G. (Ed.), *Archiv für Hydrobiologie, Organ der Internationalen Vereinigung für Theoretische und angewandte Limnologie*: Stuttgart (E. Schweizerbart’sche Verlagsbuchhandlung), 154–164.
- Neher, J., and Rohrer, E., 1958. Dolomitbildung unter Mitwirkung von Bakterien. *Eclogae Geol. Helv.*, 51:213–215.

- Pisciotta, K.A., and Mahoney, J.J., 1981. Isotopic survey of diagenetic carbonates, Deep Sea Drilling Project, Leg 63. *In* Yeats, R.S., Haq., B.U., et al., *Init. Repts. DSDP*, 63: Washington (U.S. Govt. Printing Office), 595–609.
- Resig, J.M., 1990. Benthic foraminiferal stratigraphy and paleoenvironments off Peru, Leg 112. *In* Suess, E., von Huene, R., et al., *Proc. ODP, Sci. Results*, 112: College Station, TX (Ocean Drilling Program), 263–296.
- Shipboard Scientific Party, 2003. Site 1229. *In* D'Hondt, S.L., Jørgensen, B.B., Miller, D.J., et al., *Proc. ODP, Init. Repts.*, 201, 1–78 [CD-ROM]. Available from: Ocean Drilling Program, Texas A&M University, College Station TX 77845-9547, USA. [[HTML](#)]
- Suess, E., von Huene, R., et al., 1988. *Proc. ODP, Init. Repts.*, 112: College Station, TX (Ocean Drilling Program).
- Thornburg, T.M., and Suess, E., 1990. Carbonate cementation of granular and fracture porosity: implications for the Cenozoic hydrologic development of the Peru continental margin. *In* Suess, E., von Huene, R., et al., *Proc. ODP, Sci. Results*, 112: College Station, TX (Ocean Drilling Program), 95–109.
- van Lith, Y., Warthmann, R., Vasconcelos, C., and McKenzie, J.A., 2003. Microbial fossilization in carbonate sediments: a result of the bacterial surface involvement in dolomite formation. *Sedimentology*, 50:237–245. doi:10.1046/j.1365-3091.2003.00550.x
- Vasconcelos, C., and McKenzie, J.A., 1997. Microbial mediation of modern dolomite precipitation and diagenesis under anoxic conditions (Lagoa Vermelha, Rio de Janeiro, Brazil). *J. Sediment. Res.*, 67:378–390.
- Vasconcelos, C., McKenzie, J.A., Bernasconi, S., Grujic, D., and Tiens, A.J., 1995. Microbial mediation as a possible mechanism for natural dolomite formation at low temperatures, *Nature (London, U. K.)*, 377:220–222. doi:10.1038/377220a0
- Warthmann, R., van Lith, Y., Vasconcelos, C., McKenzie, J.A., and Karpoff, A.M., 2000. Bacterially induced dolomite precipitation in anoxic culture experiments. *Geology*, 28:1091–1094. doi:10.1130/0091-7613(2000)028<1091:BDPIA>2.3.CO;2
- Wefer, G., Heinze, P., and Suess, E., 1990. Stratigraphy and sedimentation rates from oxygen isotope composition, organic carbon content, and grain-size distribution at the Peru upwelling region: Holes 680B and 686B. *In* Suess, E., von Huene, R., et al., *Proc. ODP, Sci. Results*, 112: College Station, TX (Ocean Drilling Program), 355–367.

Figure F1. Peru margin area with locations of Leg 201 sites.

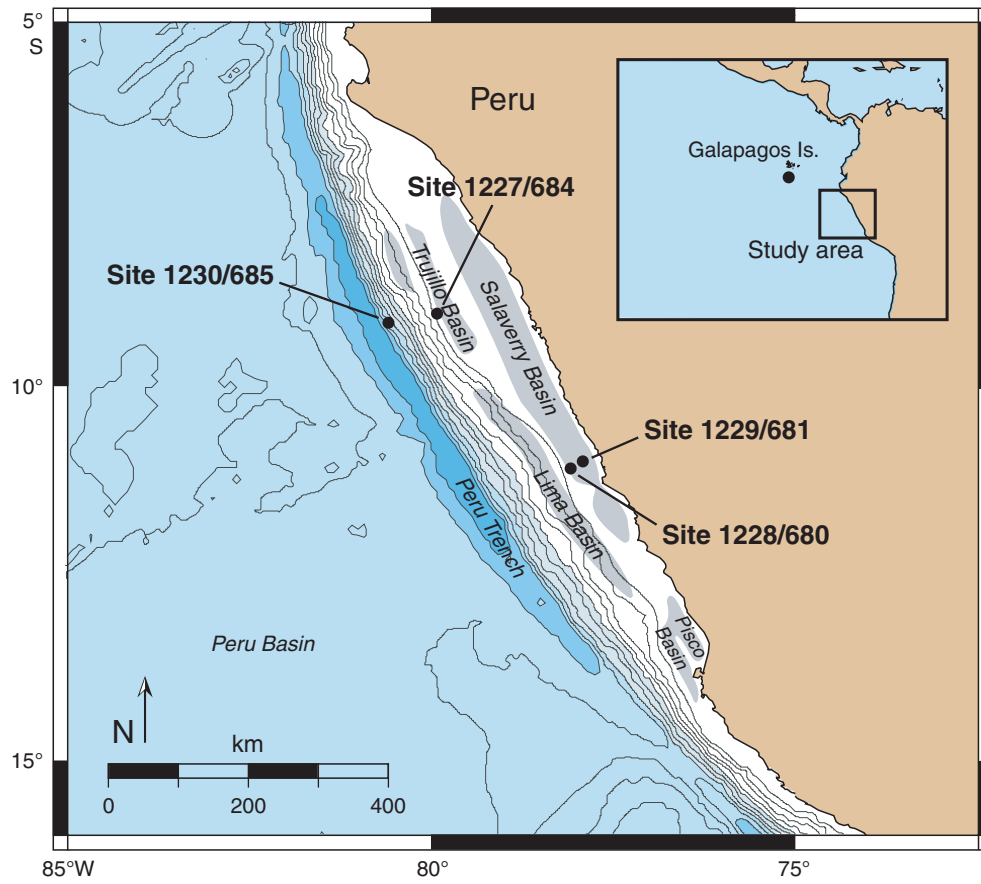


Figure F2. Lithostratigraphic profile and occurrence of dolomite at Site 1227/684. Dolomite occurs as pebbles in reworked layers or as centimeter-scale clasts at distinct horizons. In the upper 50 mbsf, barite layers are present instead of dolomite. Core photos of dolomite occurrences are arranged according to depth. TD = total depth.

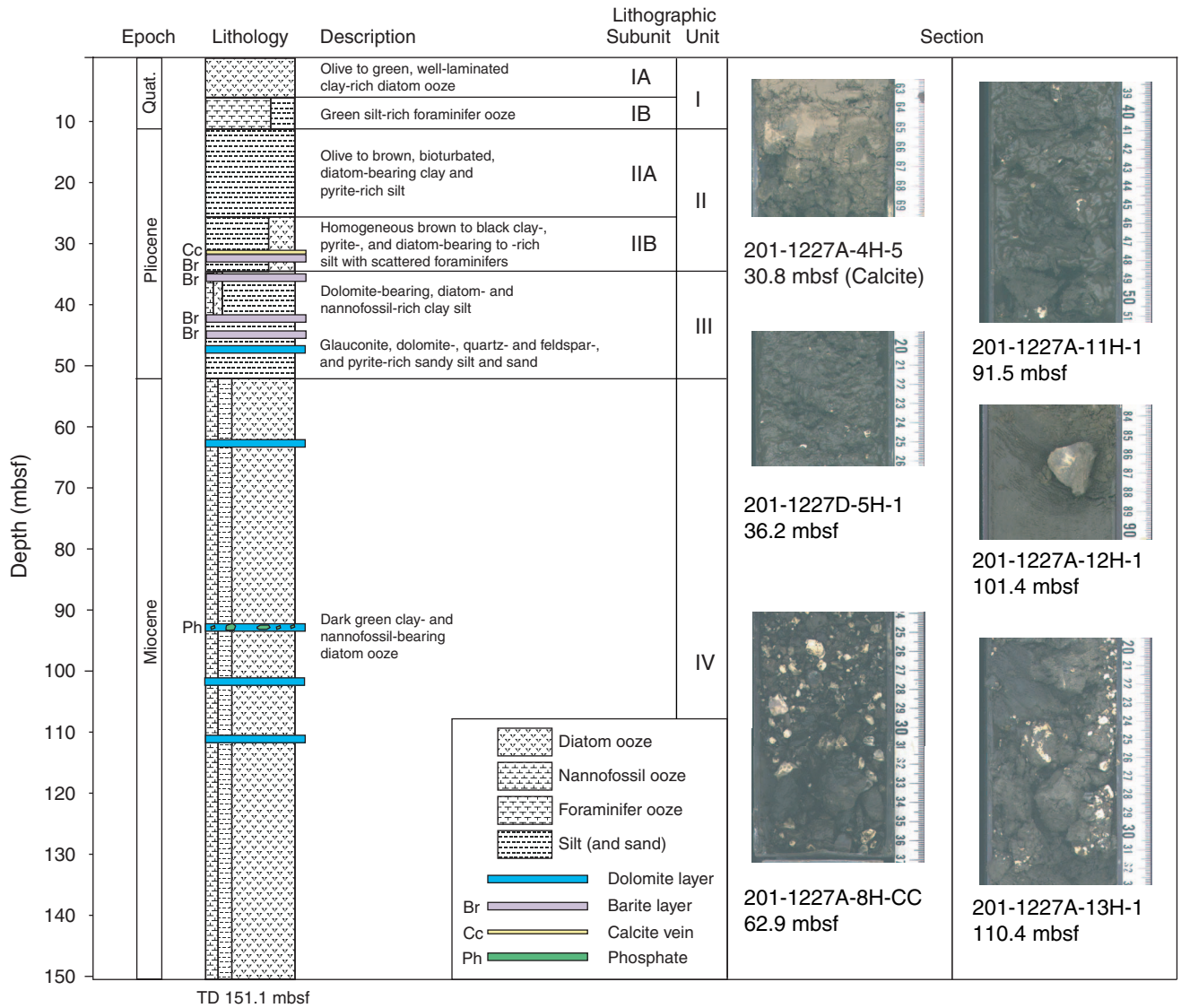


Figure F3. X-ray diffractograms of dolomite samples from Sites 1227, 1228, 1229, and 1230. Dolomite is the major compound in all samples. Narrow (104) peaks indicate very high stoichiometric ordering. Using the equation of Lumsden (1979), a slight enrichment of calcium was calculated for the dolomite phase.

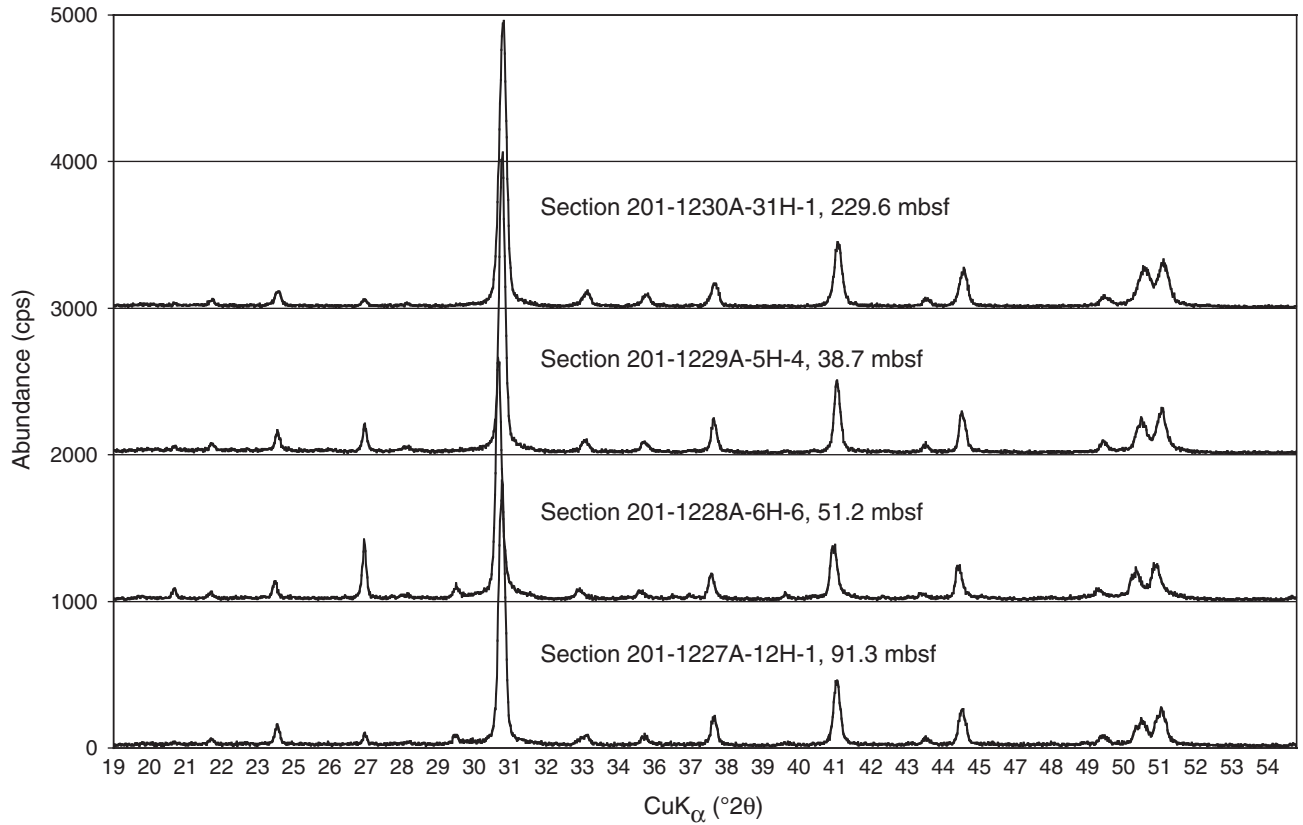


Figure F4. Lithostratigraphic profile and occurrence of dolomite at Site 1228/680. Core photos of dolomite occurrences are arranged according to depth. Dolomite layers are homogeneous and generally ~5 cm thick. TD = total depth.

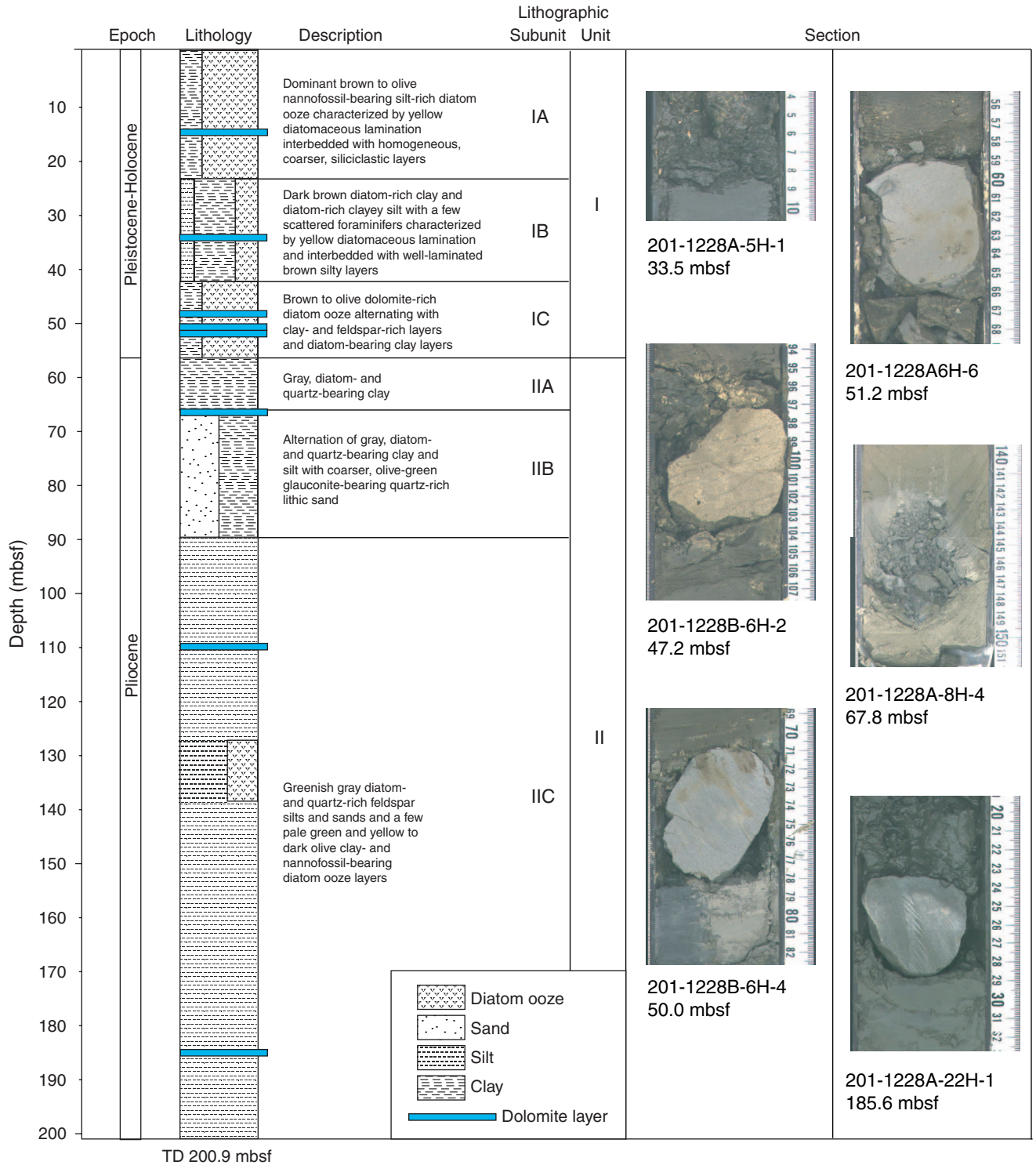


Figure F5. Lithostratigraphic profile and occurrence of dolomite at Site 1229/681. Core photos of dolomite occurrences are arranged according to depth. Dolomite layers are generally 2 to 3 cm thick and laminated. Laminae of friable dolomite occur adjacent to hard nodules or rarely within the soft sediment, as in Section 201-1229A-12H-4. TD = total depth. (Continued on next page.)

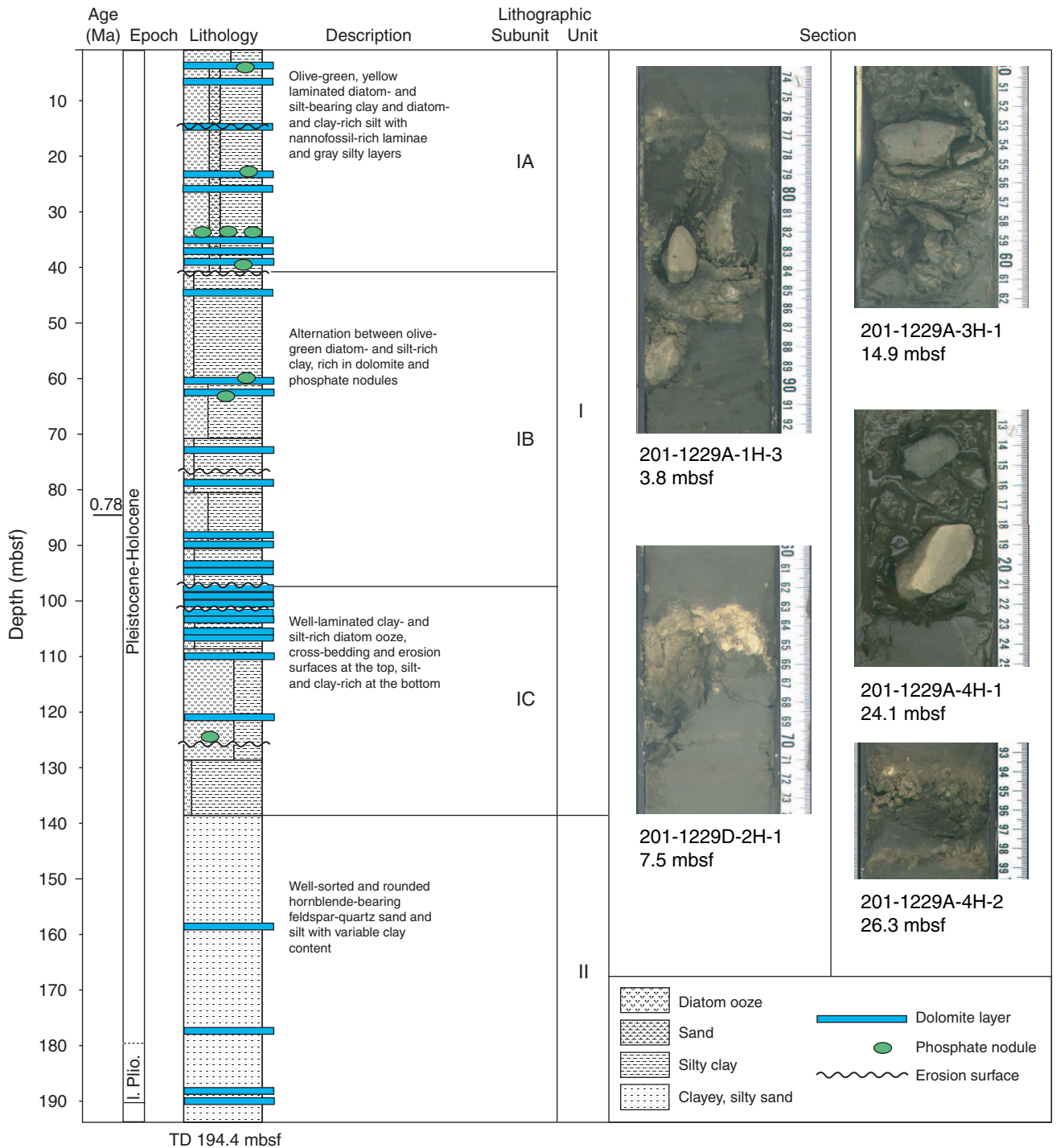


Figure F5 (continued).

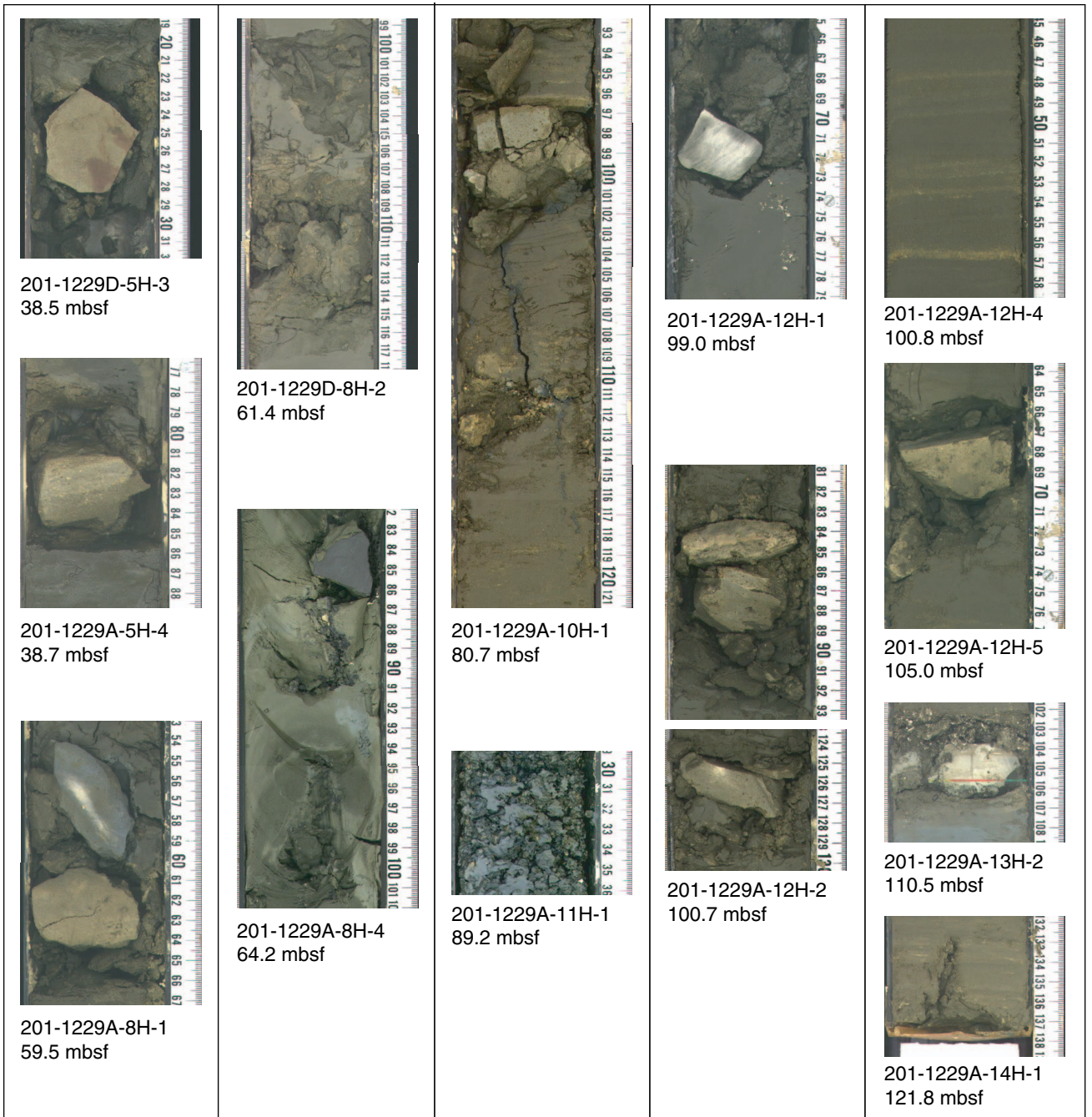


Figure F6. Lithostratigraphic profile and occurrence of dolomite at Site 1230/685. Core photos of dolomite occurrences are arranged according to depth. Dolomite occurs as breccias and hard lithified layers ~230 mbsf. Only one dolomite layer is present at 7 mbsf.

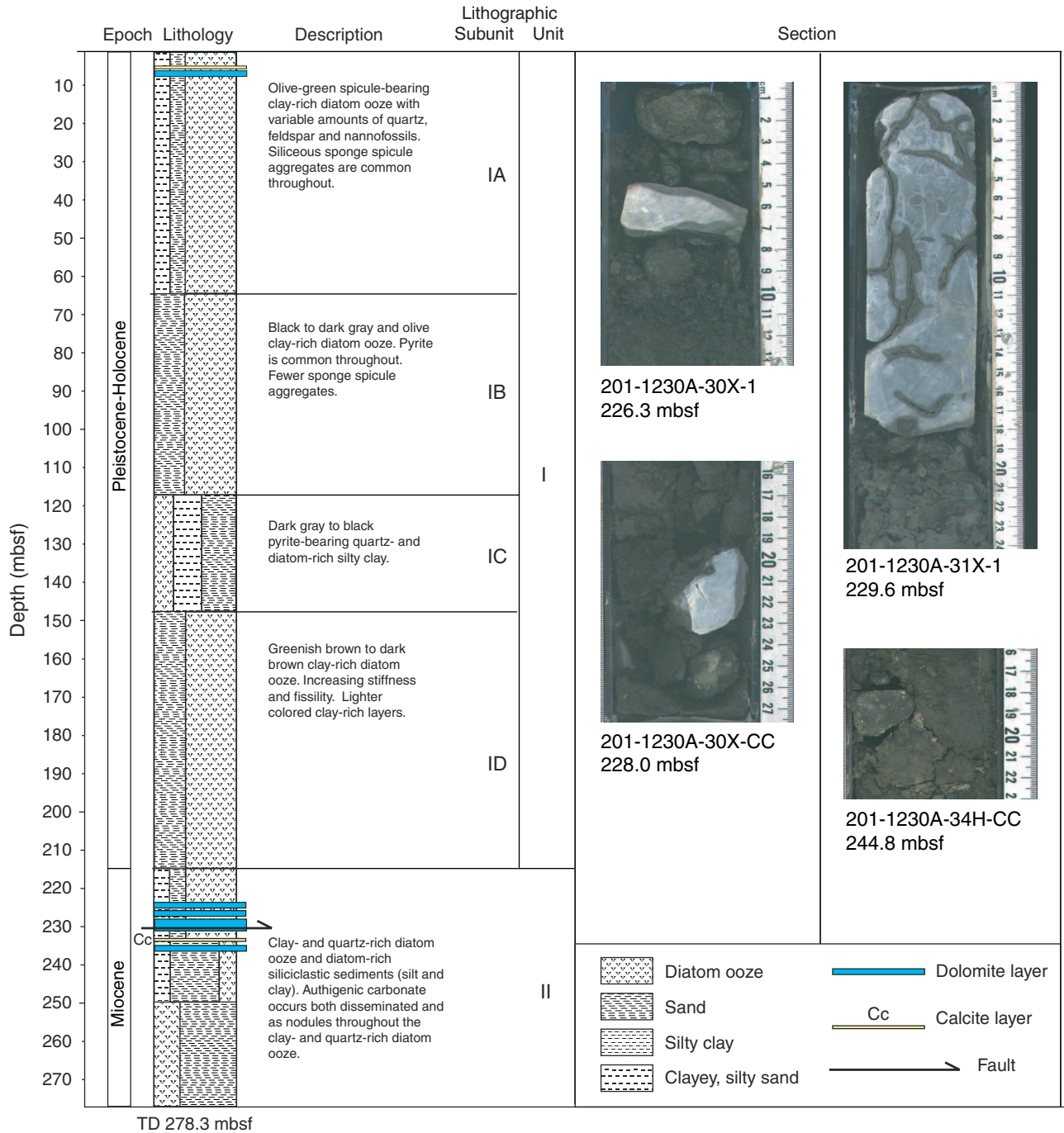
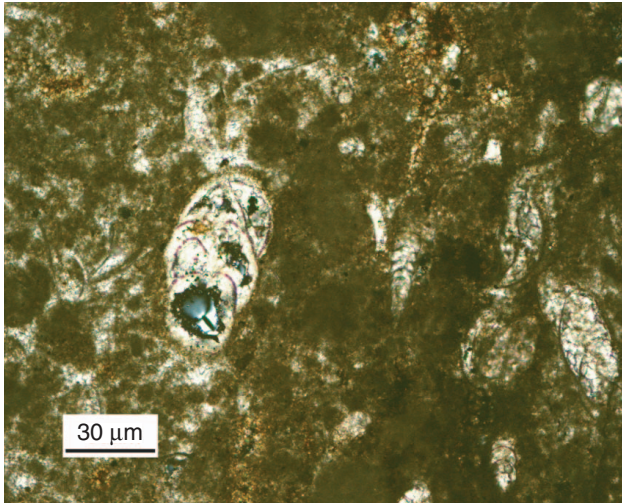
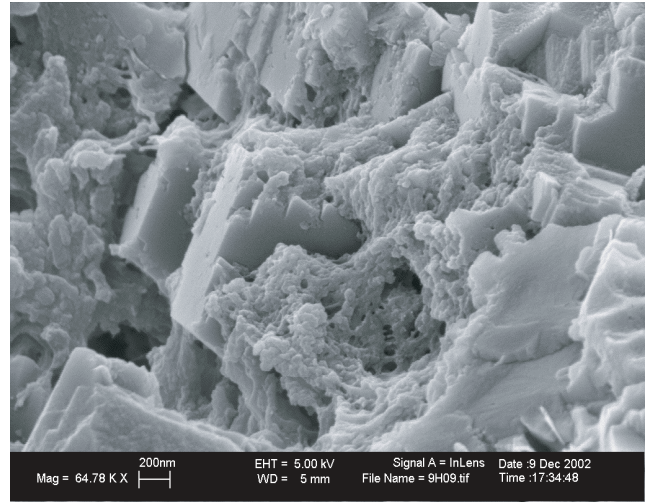


Plate P1. A. Foraminifers in dolomicritic groundmass. Foraminifer chambers are partially filled with calcite or dolomite cement (Sample 201-1227A-8H-CC, 30–36 cm; 62.9 mbsf). B. Groundmass consisting of euhedral decimicron-size dolomite rhombs (Sample 201-1227A-12H-1, 85–88 cm; 101.4 mbsf). C. Curve-shaped crystal surfaces in coarse-grained dolomite (Sample 201-1227A-13H-1, 28–30 cm; 110.4 mbsf) are probably the result of cemented skeletal fragments. D. Foraminiferal test in a microsparitic dolomite groundmass. The perforate structure of the foraminiferal test is well preserved and probably still consists of biogenic calcite, whereas chambers show coarse fringes of isopachous, blocky (probably dolomitic) cement on the inside (Sample 201-1227A-13H-1, 28–30 cm; 110.4 mbsf).

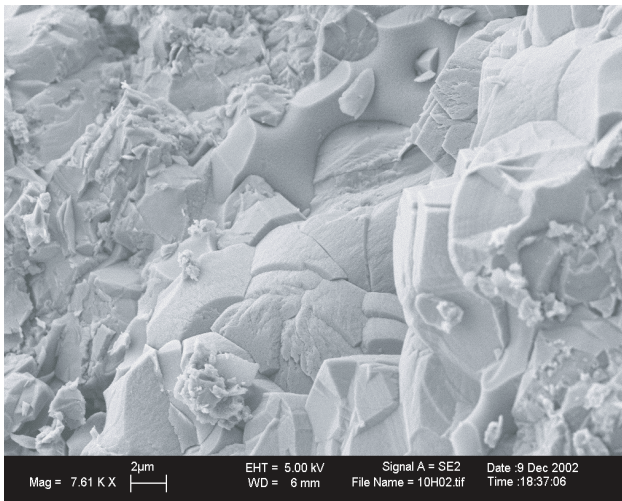
A



B



C



D

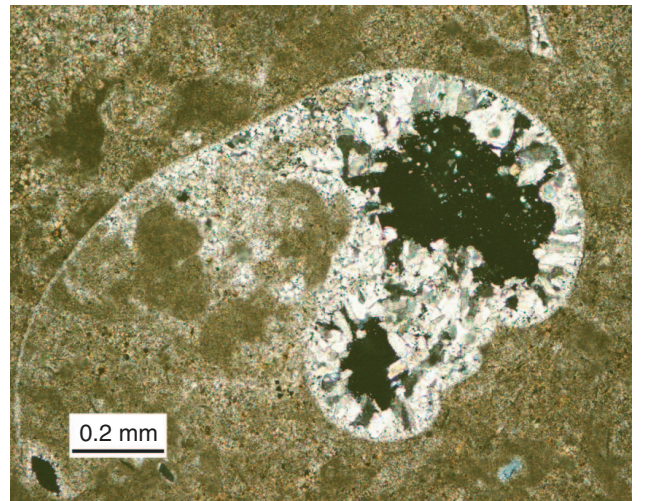
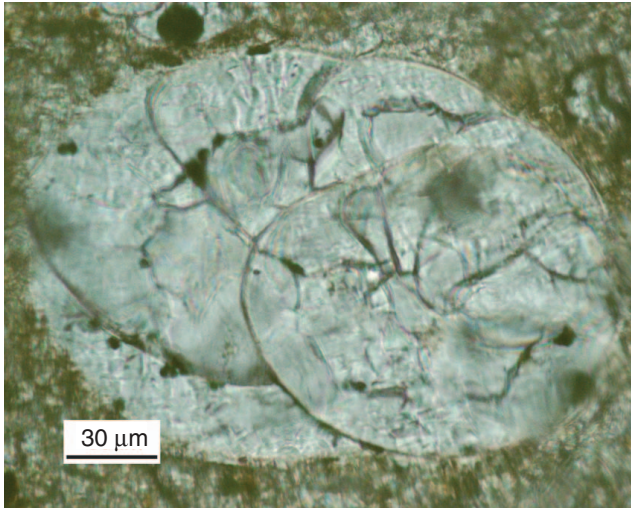
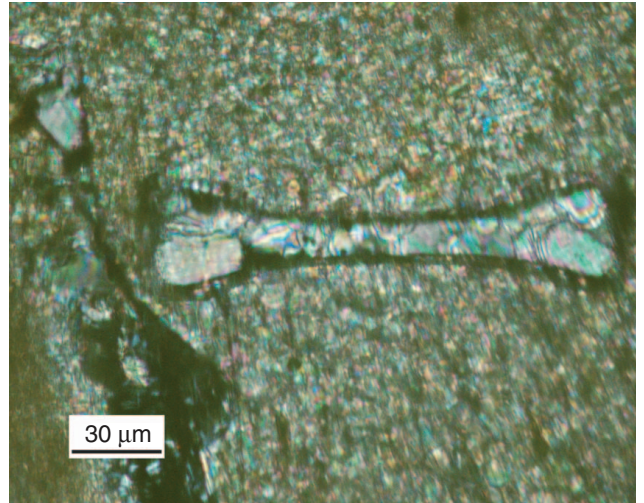


Plate P2. A. Foraminiferal test entirely filled with coarse dolomitic cement (Sample 201-1227A-13H-1, 28–30 cm; 110.4 mbsf). B. Cross section of diatom frustule filled with coarse dolomite cement (Sample 201-1227A-13H-1, 28–30 cm; 110.4 mbsf). C. Framboidal pyrite and needle-shaped unknown mineral (Sample 201-1227A-12H-1, 79–91 cm; 101.4 mbsf). D. Orange luminescent dolomicrosparite. The foraminiferal tests show low luminescence, whereas cement rims are zoned around the cavities (Sample 201-1227A-12H-1, 85–88 cm; 101.4 mbsf).

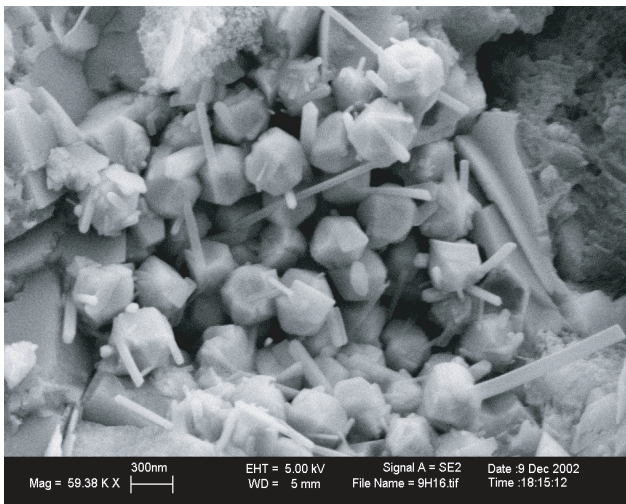
A



B



C



D

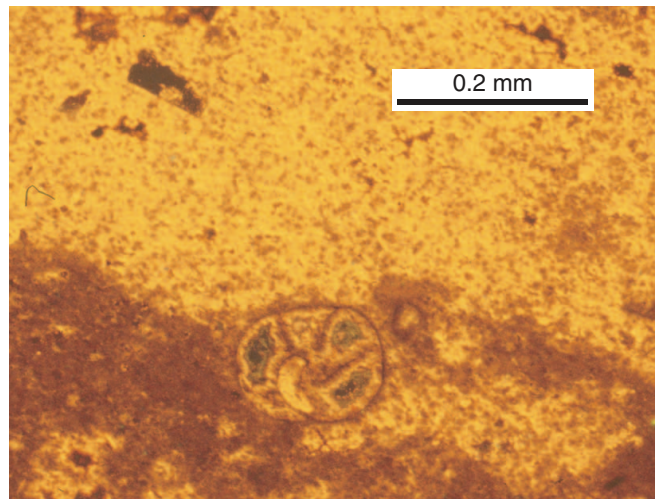


Plate P3. A. Decimicron-size dolomite rhomb. Fine-grained minerals in the bottom right area could not be identified by EDX (Sample 201-1228A-5H-1, 5–10 cm; 33.45 mbsf). B. Euhedral dolomicrosparite (Sample 201-1228A-5H-1, 5–10 cm; 33.45 mbsf). C. Porous dolomicrosparite. Foraminiferal tests mostly form solution cavities (Sample 201-1228A-5H-1, 5–10 cm; 33.45 mbsf). D. Foraminiferal test in dolomicrosparite matrix under cross-polarized light shows growth of syntaxial calcite. Direction of extinction indicates that the cement is in crystallographic continuity with the test (Sample 201-1228B-6H-2, 97–101 cm; 50 mbsf).

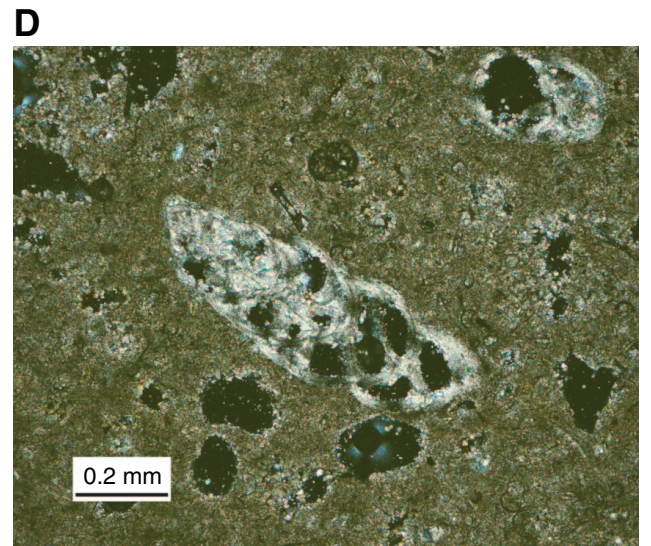
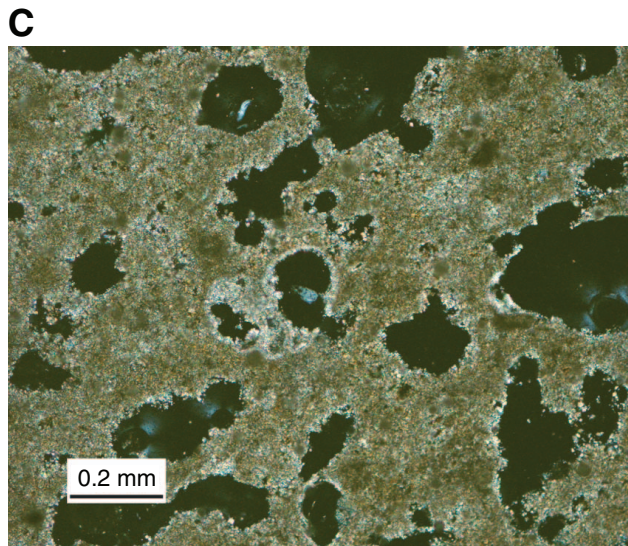
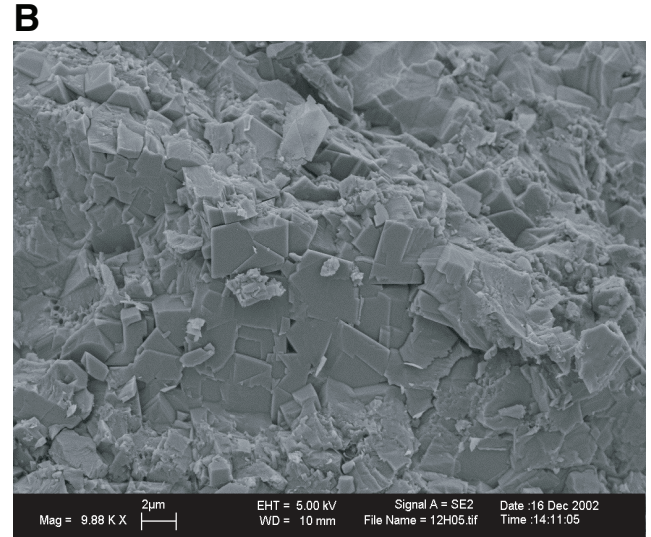
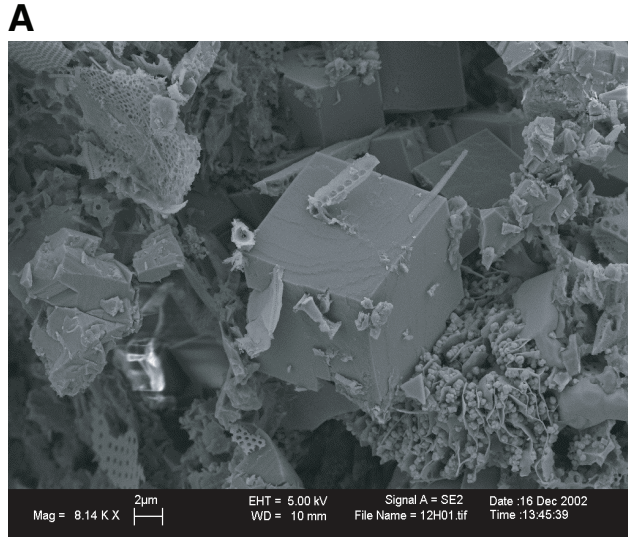


Plate P4. A. Foraminiferal test with partially preserved original wall structure and isopacheous fringes of blocky, probably dolomitic, cement on the inside (Sample 201-1228B-6H-2, 97–101 cm; 50 mbsf). B. Quartz-rich dolomicrosparite (Sample 201-1228A-22H-1, 22–26 cm; 185.6 mbsf). C. Siliceous tube (center) is well preserved but enveloped by a decimicron-size dolomite rhomb (Sample 201-1228A-5H-1, 5–10 cm; 33.45 mbsf). D. Well-preserved diversely shaped diatom frustules. One of them (center) is enveloped by an euhedral dolomite rhomb (Sample 201-1228A-8H-4, 144–150 cm; 67.8 mbsf).

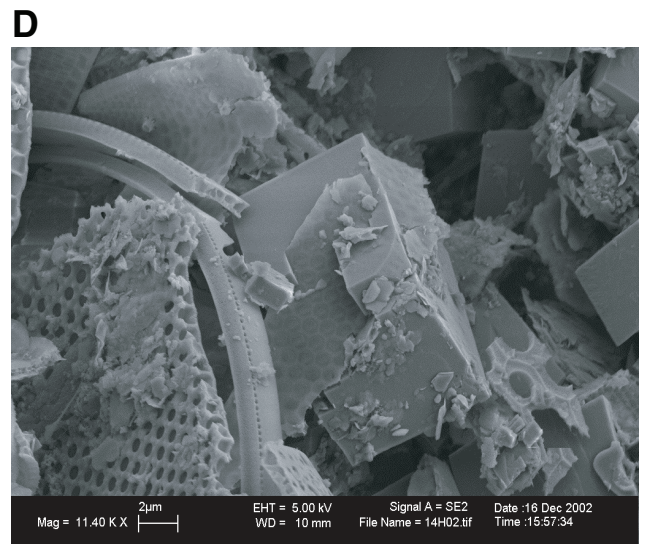
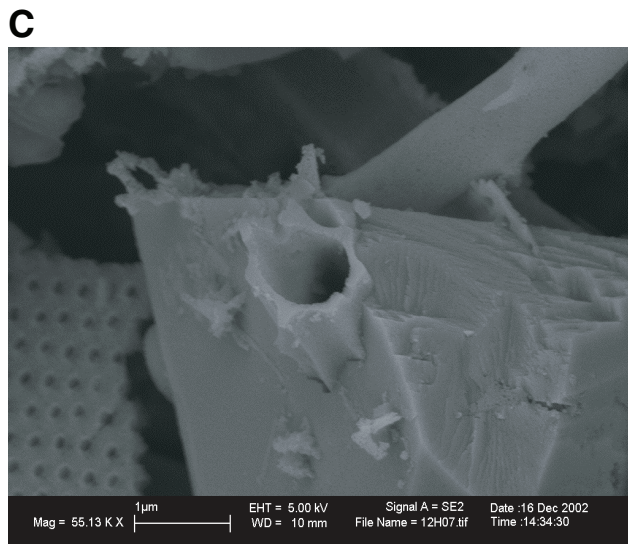
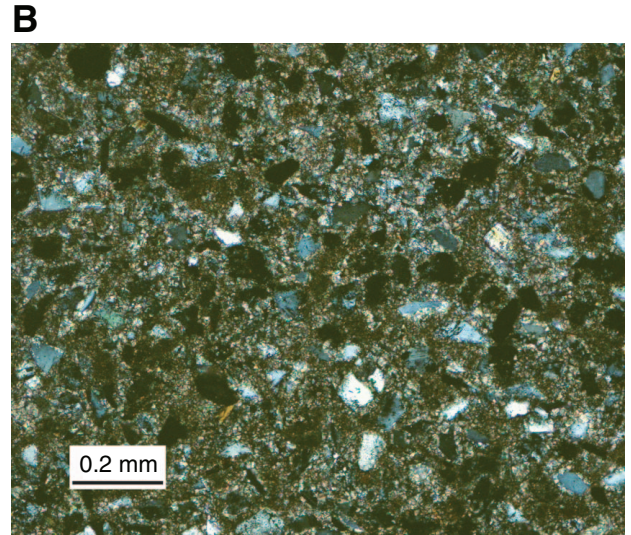
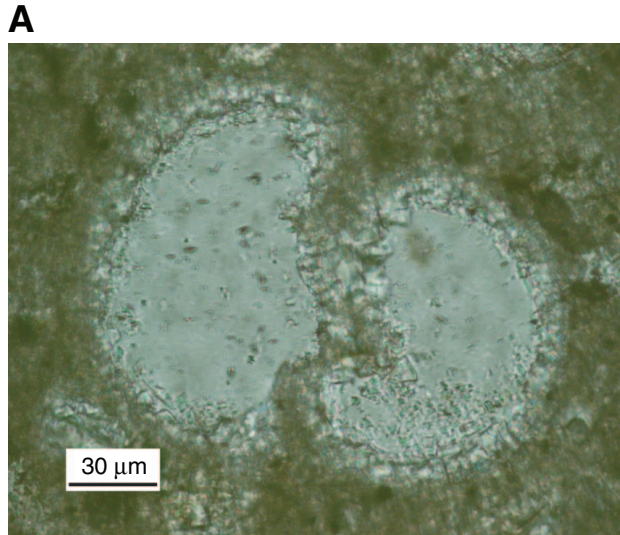
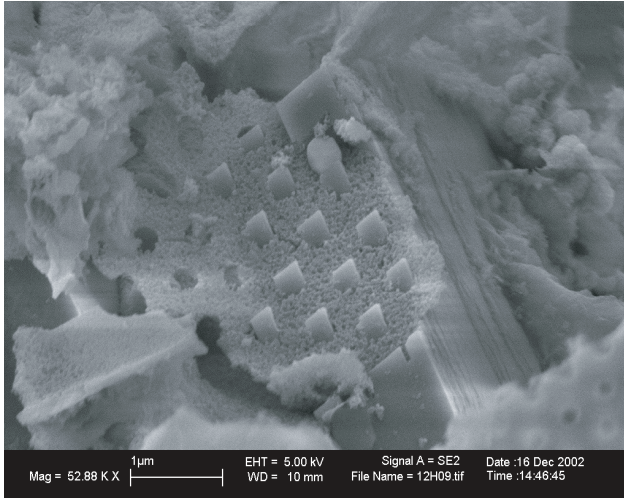
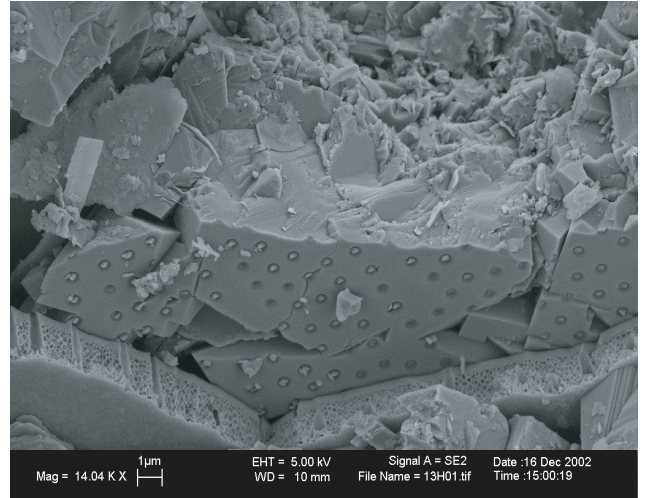


Plate P5. A. Diatom frustule more strongly edged than surrounding diatom frustules. Dolomite rhombs growing inside the pores show the same crystallographic orientation (Sample 201-1228A-5H-1, 5–10 cm; 33.45 mbsf). B, C. Replication of diatom frustules on surrounding dolomite (Sample 201-1228A-6H-6, 62–70 cm; 51.2 mbsf). D. Framboidal pyrite growing in the pore space of a diatom frustule (Sample 201-1228A-6H-6, 62–70 cm; 51.2 mbsf).

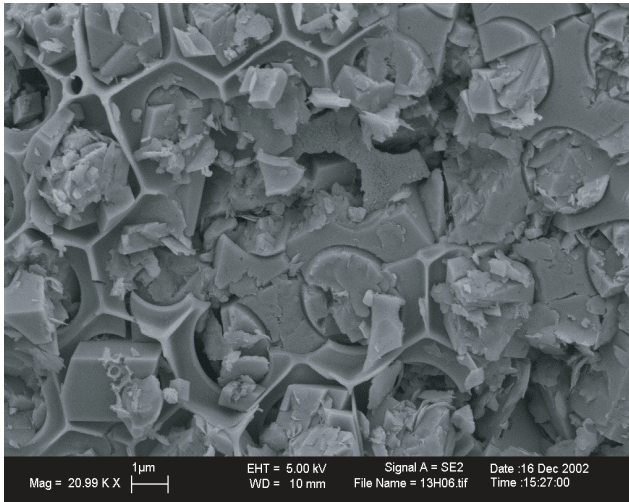
A



B



C

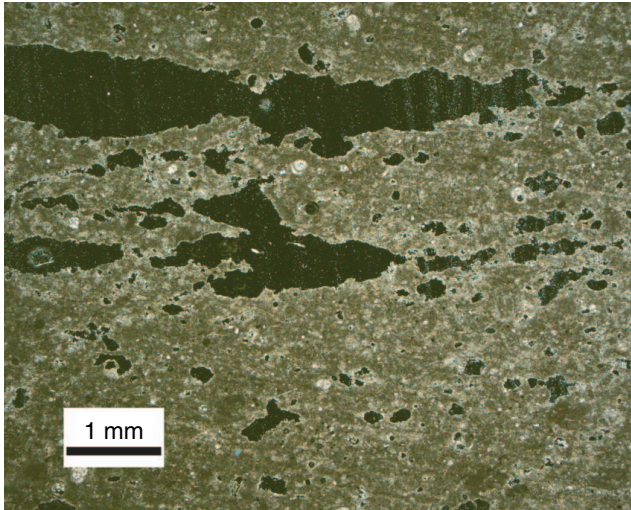


D

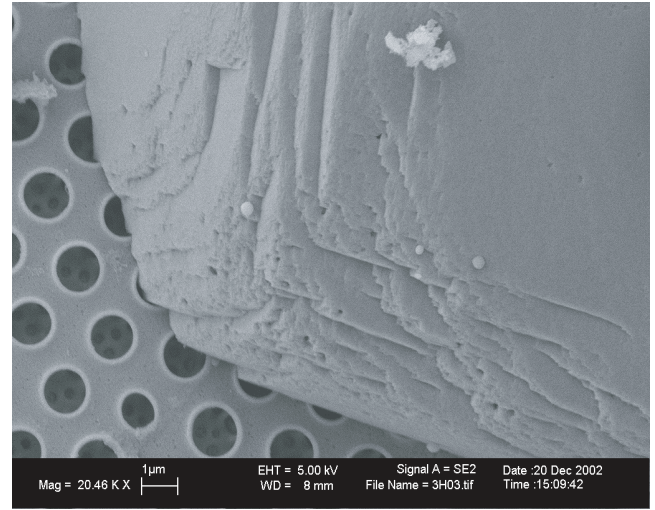


Plate P6. A. Elongate pores parallel to lamination occurring only in more friable laminae (Sample 201-1229A-11H-1, 31–34 cm; 89.2 mbsf). B. Large centimicron-size dolomite rhombs occur at only 7.5 mbsf at Site 1229. It is distinguished from all other dolomite rhombs by etched corners (Sample 201-1229D-2H-1, 71–72 cm; 7.5 mbsf). C, D. Foraminiferal test filled with fringes of fibrous calcite cement partially replacing the original test. A second generation of decimicron-size, probably dolomitic, blocky cement is filling the central cavity. C. Sample 201-1229A-12H-5, 68–69 cm; 105.1 mbsf. D. Sample 201-1229A-12H-5, 68–69 cm; 105.1 mbsf.

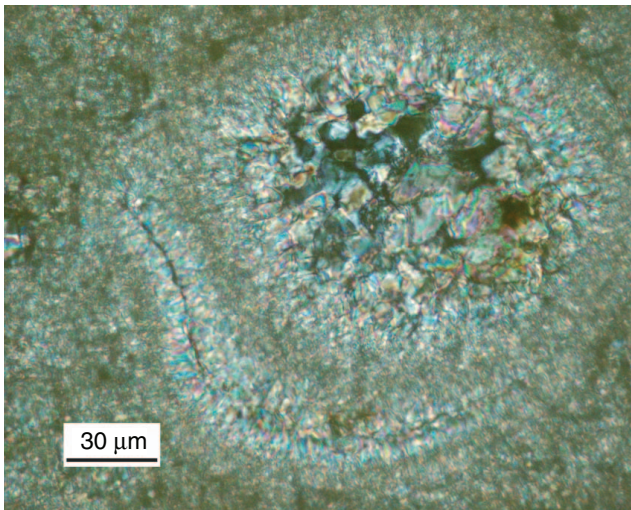
A



B



C



D

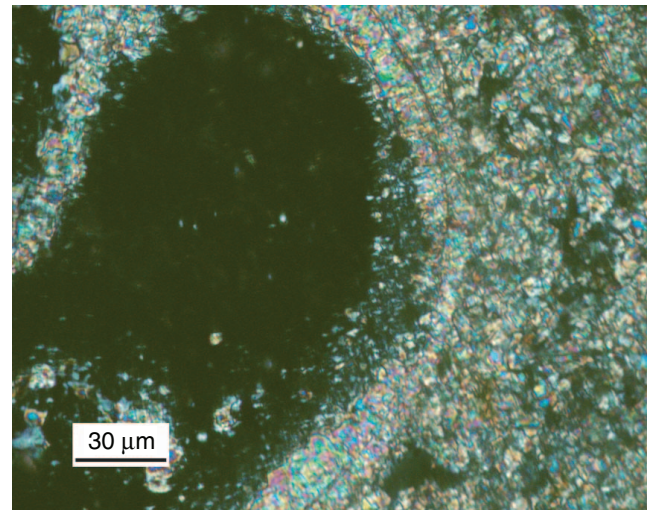
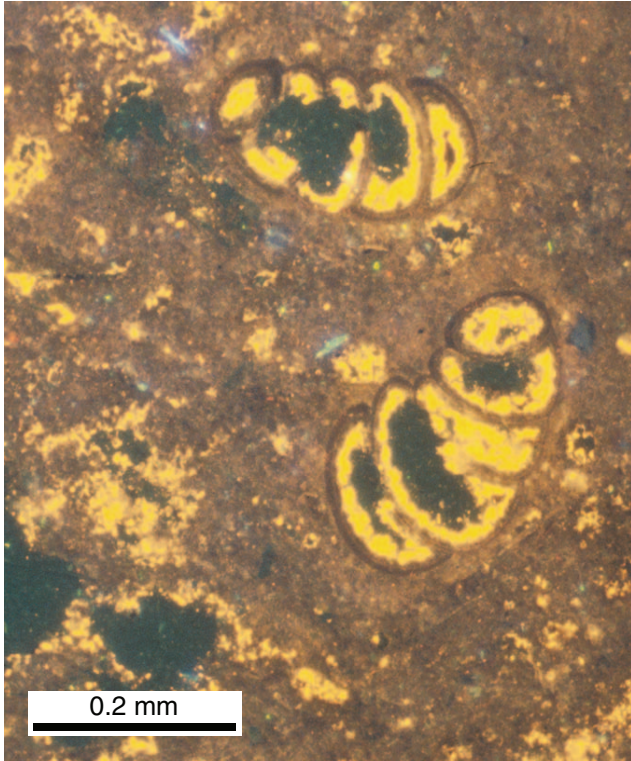
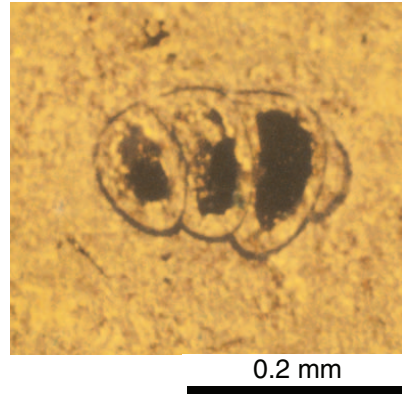


Plate P7. A. Cathode luminescence reveals poorly luminescent calcitic foraminiferal tests with thin seams of fibrous calcite cement on the inside of the chambers followed by a coarse rim of bright luminescent blocky dolomite cement (Sample 201-1229A-12H-2, 86–88 cm; 100.8 mbsf). B. Foraminiferal test without calcite cement (Sample 201-1229A-4H-2, 95–96 cm; 26.3 mbsf). C. Like A, but cavities are completely filled with luminescent blocky cement (Sample 201-1229A-12H-1, 64–65 cm; 99.0 mbsf).

A



B



C

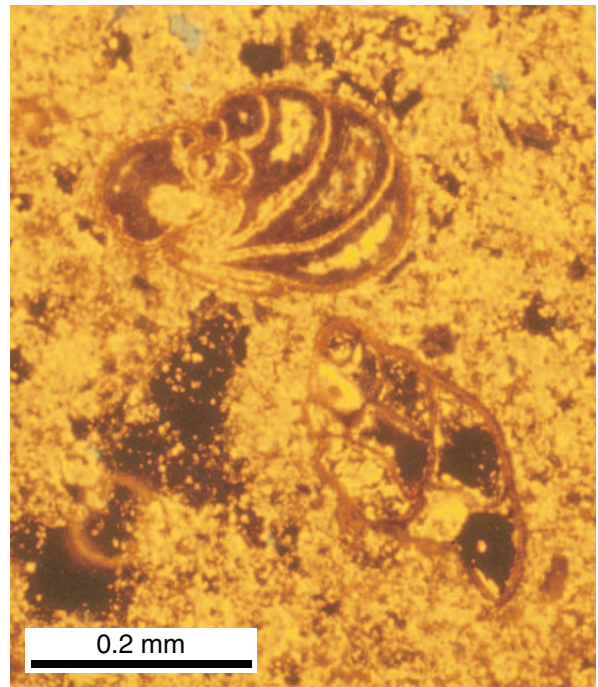


Plate P8. Sample 201-1229A-8H-1, 55–64 cm; 59.5 mbsf. **A, B.** Thick-walled perforate foraminiferal test surrounded by an equigranular layer of decimicron-size euhedral dolomite rhombs. **C, D.** Replica of perforate surface of the foraminiferal test on dolomite rhombs.

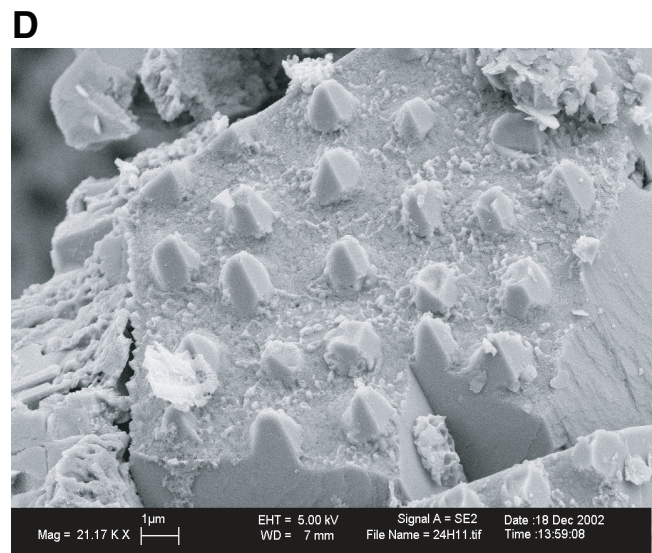
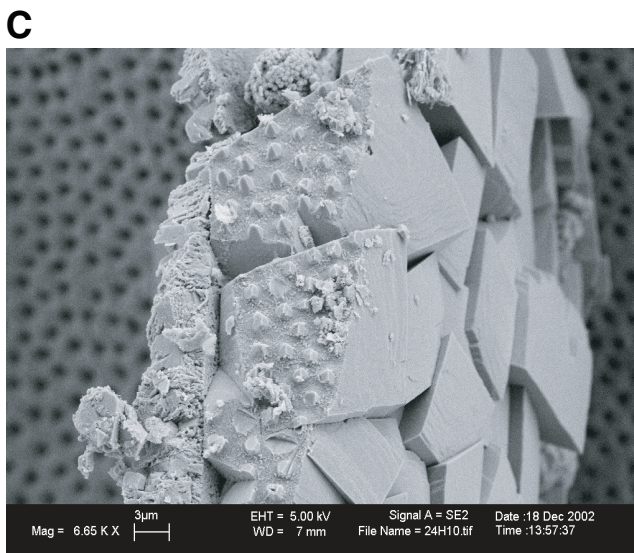
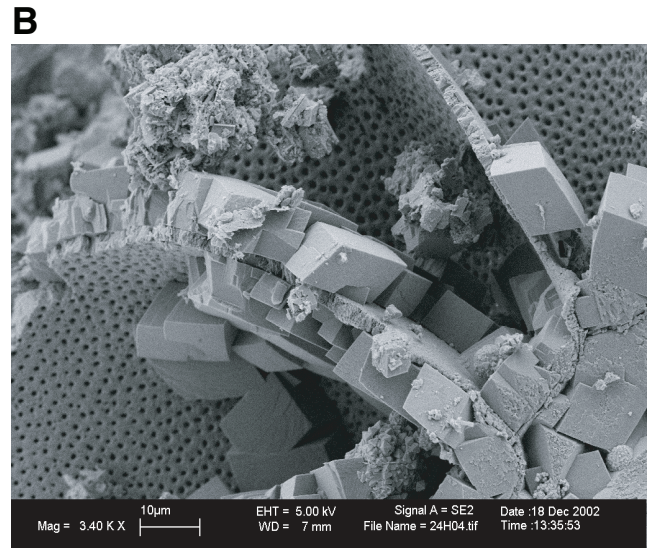
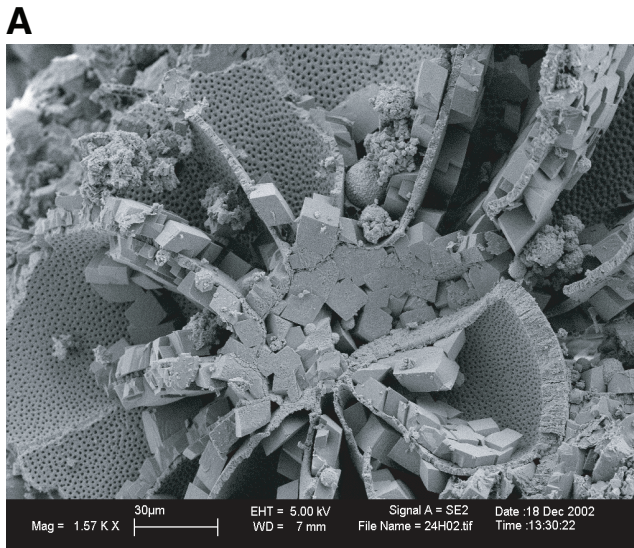
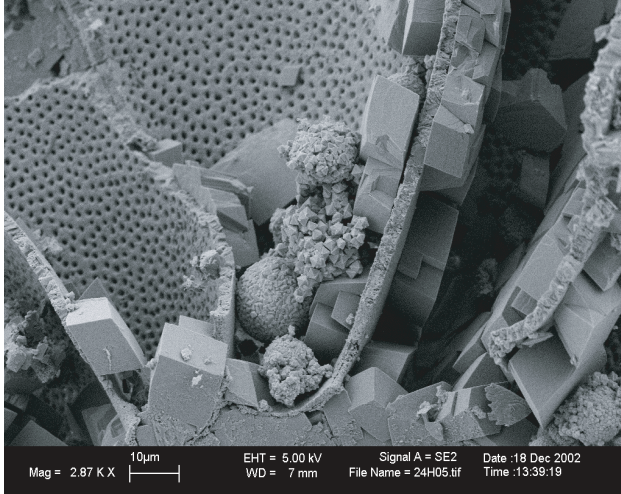
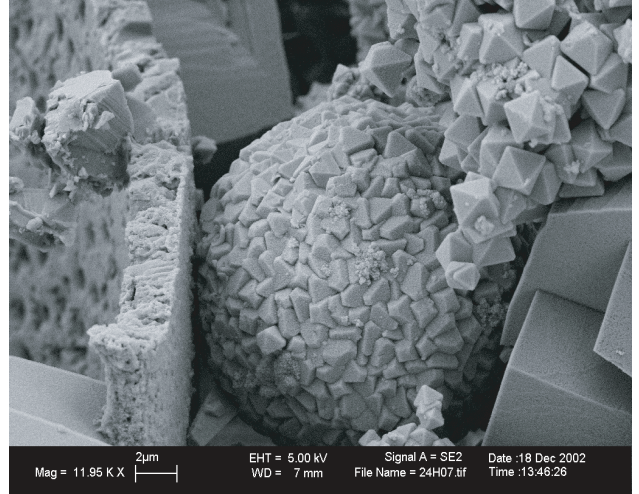


Plate P9. A, B. Perfectly shaped pyrite framboids growing in the pore space between the dolomite rhombs and, therefore, postdating the precipitation of dolomite (Sample 201-1229A-8H-1, 55–64 cm; 59.5 mbsf). C. Cross section of diatom-rich dolomicrosparite (Sample 201-1229A-10H-1, 133–136 cm; 80.7 mbsf). D. Diatom filled with coarse blocky dolomite cement (Sample 201-1229A-4H-1, 18–19 cm; 24.1 mbsf).

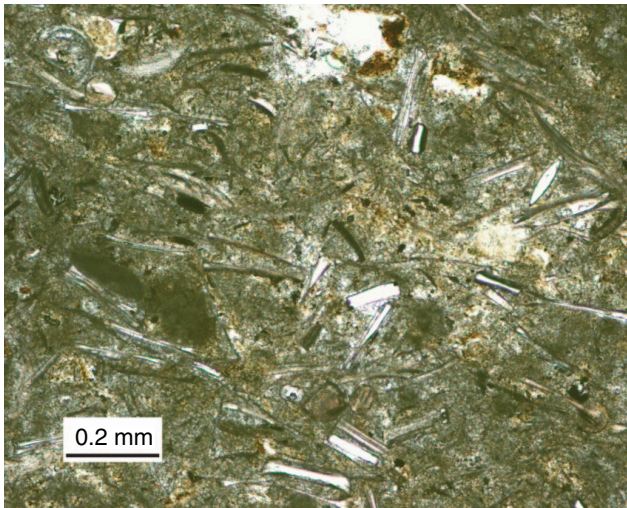
A



B



C



D

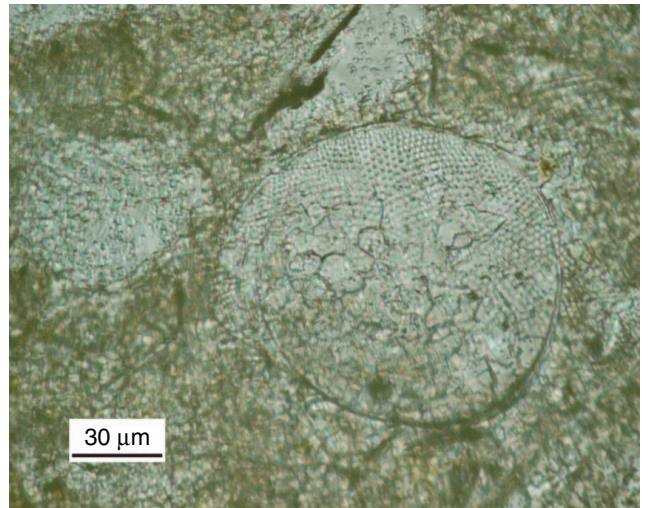


Plate P10. Dolomite growing into the porous structure of the diatom frustules. **A.** Sample 201-1229A-4H-1, 18–19 cm; 24.1 mbsf. **B–D.** Sample 201-1229A-12H-1, 64–65 cm; 99.0 mbsf.

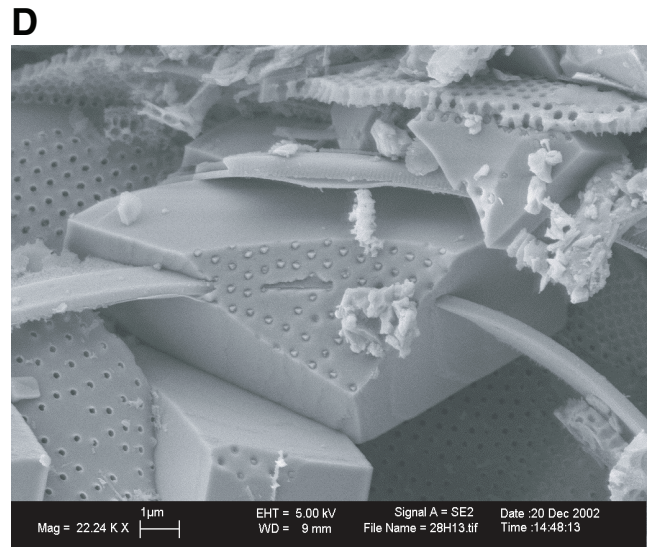
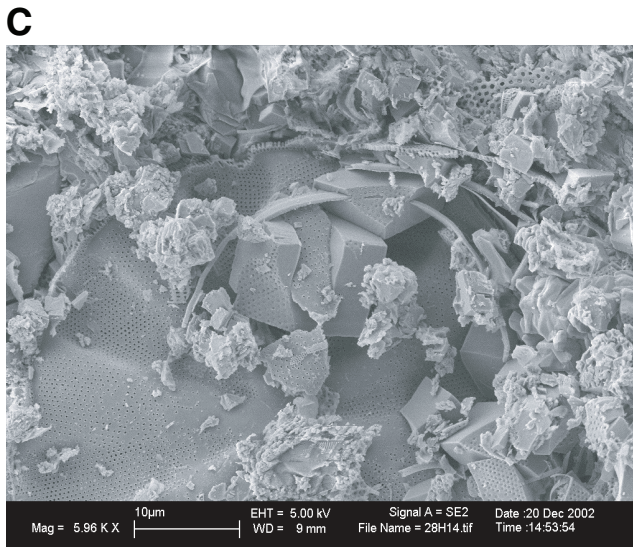
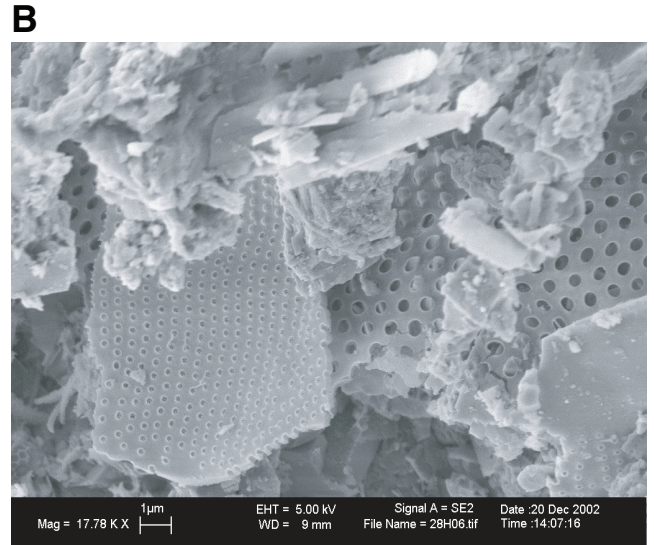
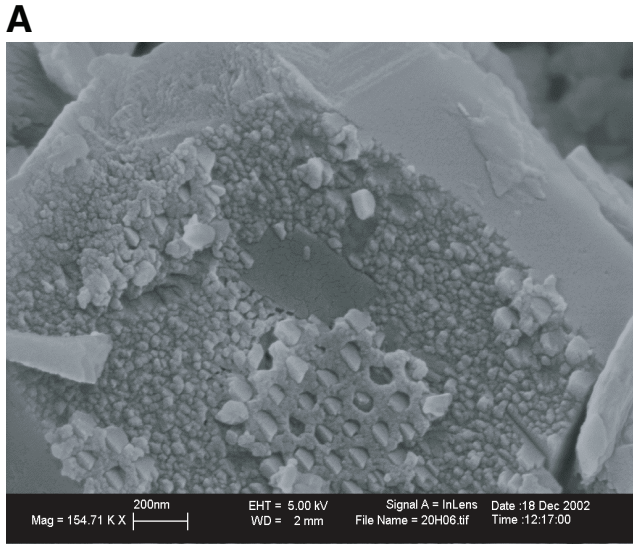


Plate P11. A. Strongly etched and partially dissolved skeletal fragment, which is not completely encased by growing dolomite (Sample 201-1229A-12H-1, 64–65 cm; 99.0 mbsf). B. Clasts of a dolomitic breccia consisting of subhedral dolomite crystals (Sample 1230A-30X-1, 0–5 cm; 226.3 mbsf). C. Cathode luminescence revealing zonation of the rhombs (Sample 201-1230A-30X-1, 0–5 cm; 226.3 mbsf).

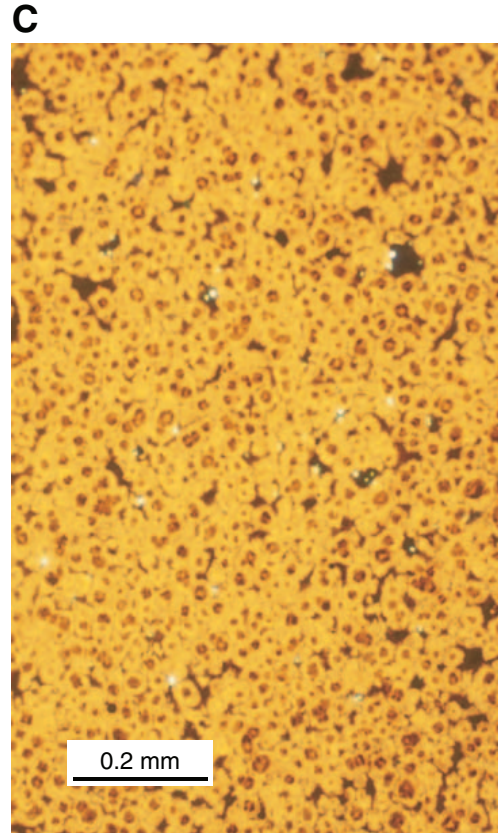
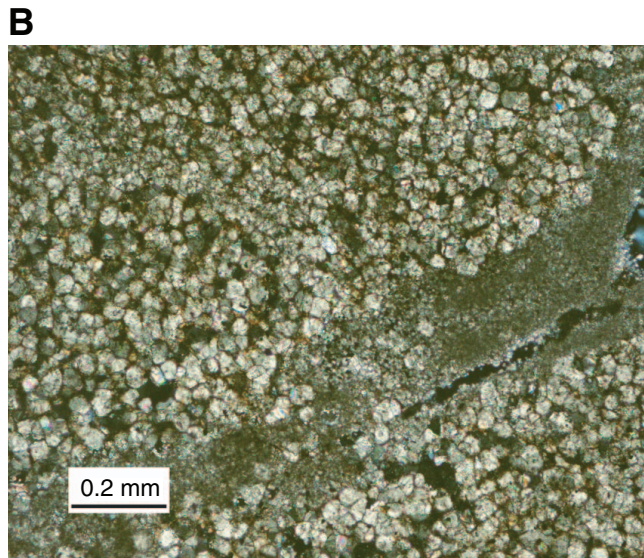
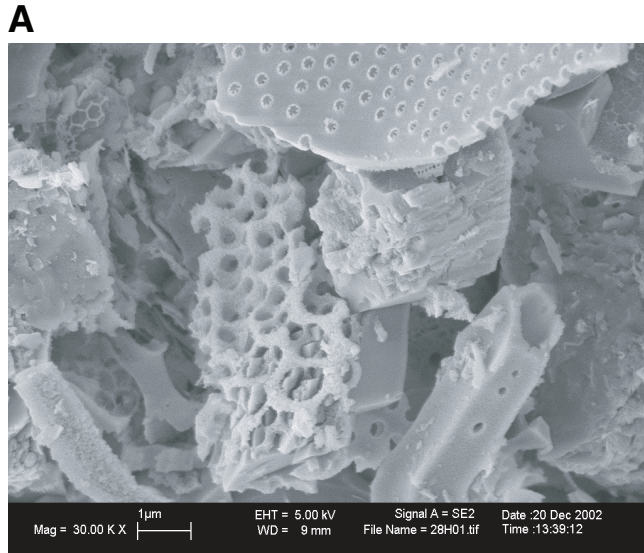
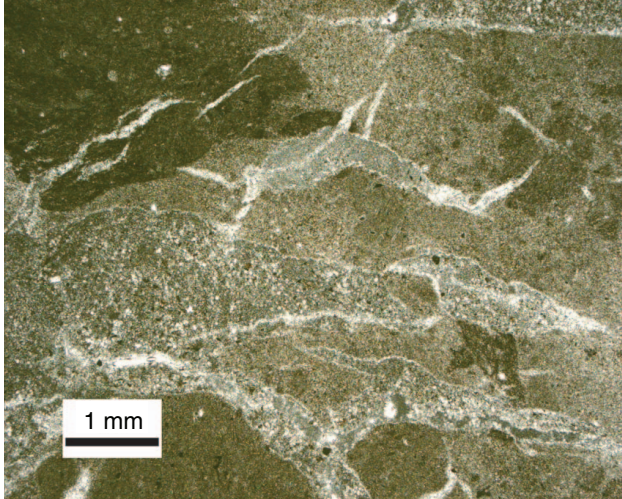
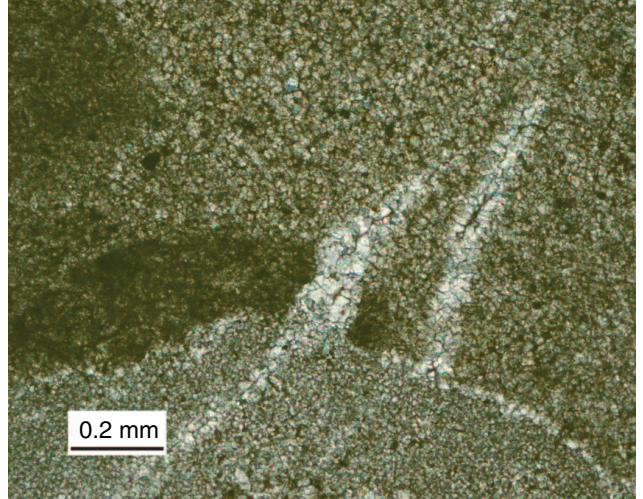


Plate P12. A, B. Dolomite breccia showing areas of dolomitic matrix in-fill and coarse cemented veins (Sample 201-1230A-31X-1, 0–19 cm; 229.6 mbsf). Anhedrally dolomite of coarse sparitic areas with almost perfect hexagonal shape. **C.** Sample 201-1230A-30X-1, 0–5 cm; 226.3 mbsf. **D.** Sample 201-1230A-31X-1, 1–19 cm; 229.6 mbsf.

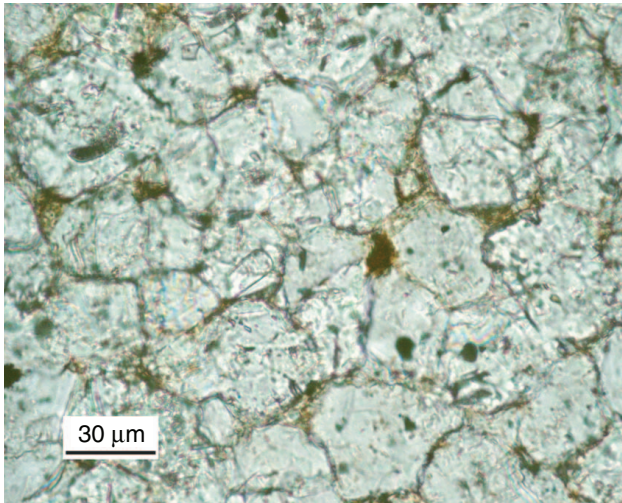
A



B



C



D

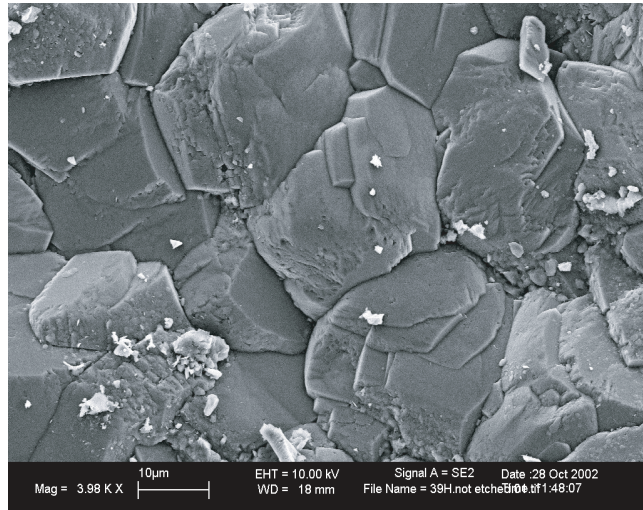
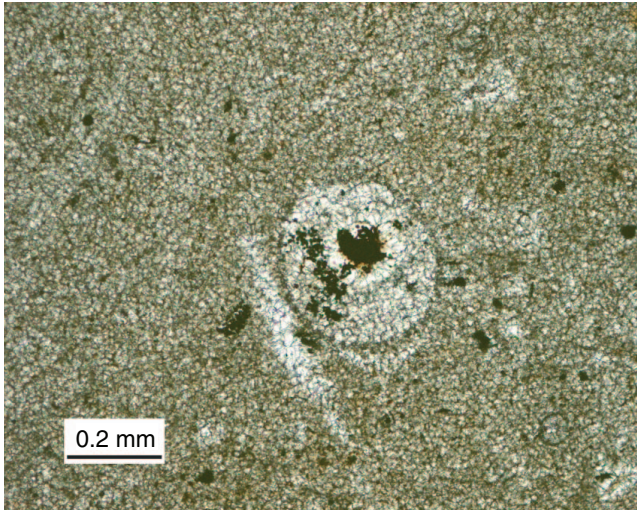
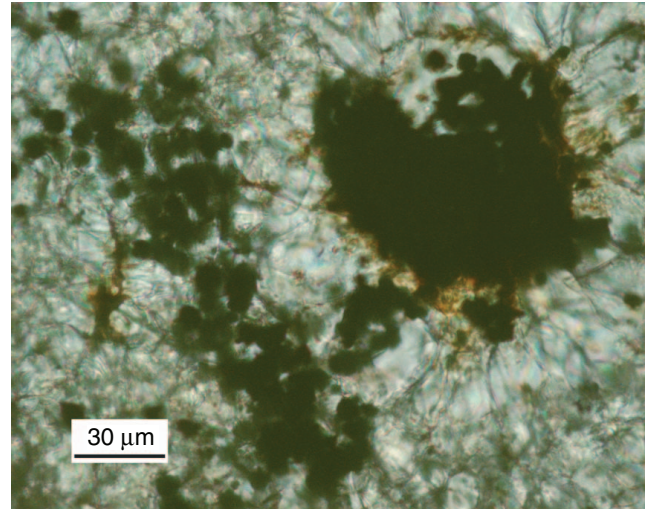


Plate P13. Sample 201-1230A-31X-1, 0–19 cm; 229.6 mbsf. **A, B.** Strongly replaced fossil (foraminifer?) showing concentric rim structure with pyrite filling the central cavity (cross-polarized light). **C, D.** Cathode luminescence microscopy reveals darker crystals in the clasts and brighter luminescence in the matrix/cement between the clasts. Both generations of cement are clearly separated by a bright yellow luminescent rim surrounding all parts of the clast. Crystals in the clast must, therefore, predate the cementation of the space between the clasts. The latter was formed during several generations of infill and cementation during deformation, leaving a central cavity with fine pyrite precipitates.

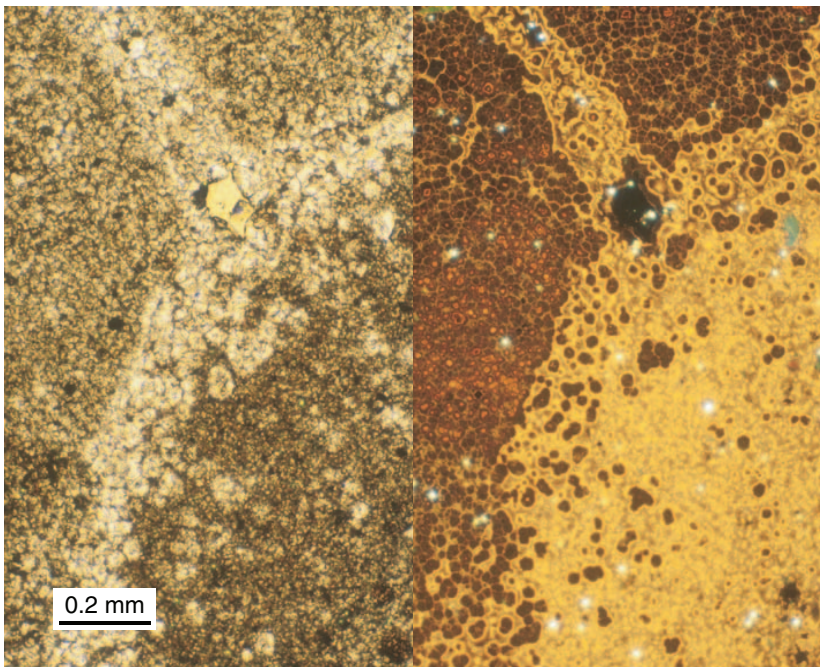
A



B



C



D

